2003

Determination of the Viscoelastic Properties of General Anisotropic Materials

Anish Sen Senan

DETERMINATION OF THE VISCOELASTIC PROPERTIES OF GENERAL ANISOTROPIC MATERIALS

By

Anish Sen Senan

B.Tech. Kerala University (India) 1998

A THESIS

Submitted in Partial Fulfillment of the

Requirements for the Degree of

Master of Science

(in Mechanical Engineering)

The Graduate School

The University of Maine

December, 2003

Advisory Committee:

Michael Peterson, Associate Professor of Mechanical Engineering, Advisor

Donald Grant, R.C. Hill Professor and Chairman of Mechanical Engineering

Senthil Vel, Assistant Professor of Mechanical Engineering

William Davids, Assistant Professor of Civil Engineering

DETERMINATION OF THE VISCOELASTIC PROPERTIES OF GENERAL ANISOTROPIC MATERIALS

By Anish Sen Senan

Thesis Advisor: Dr. Michael Peterson

An Abstract of the Thesis Presented
in Partial Fulfillment of the Requirements for the
Degree of Master of Science
(in Mechanical Engineering)
December, 2003

Elastic properties are rarely sufficient in order to evaluate the condition of a composite material. Knowledge of the viscoelastic properties is very critical for design purposes, for they directly characterize damping. Damping related measurements in the material provides information about the degree of cross-linking and crystallinity of the polymer. For metals, damping may be related to dislocation motion among other characteristics. For composite materials, in general the interphase and the matrix dominate the damping of the material. Ultrasonic measurement of damping gives a non-destructive measure of strength of composite materials. This thesis considers damping characteristics of polymer matrix composites as well as reinforced carbon-carbon (RCC). These characteristics represent perhaps the best hope of developing a true index of state or damage tensor for composite materials. For polymer matrix composites the damping and elastic properties can be combined with either temperature or pressure to characterize the interatomic potentials in the matrix. This is the closest to a non-destructive measure of strength that is likely. By describing cross linkage and

crystallinity this measure also provides insight into many of the most important degradation mechanisms. Part of this research looks into the recovery of stiffness tensor, material symmetry and principal axis. Damping is measured along this principal axis. It is also interesting to note that the damping is affected by oxidation, second part of this thesis looks into the oxidation effects of damping in RCC. Optimization routine is developed to solve Christoffel's equation to recover the material stiffness tensor. Method to determine the initial guesses for the optimization routine is also developed in this thesis. An ultrasonic microscope with immersion transducers is used to extract data from samples. Oxidation is carried out in a tube furnace run at 700°C. Stiffness tensors for the samples are recovered from the measured data using a routine applying the solution to the Christoffel's equation. Recovered stiffness tensors show satisfactory results. The orientation of the recovered stiffness tensors is very close to the material axis. Damping is measured with this variability. The variability in repeatability of damping measurements is less than 10%. Oxidation data obtained followed the initial assumptions and can be used for designing if damping accuracy can be improved.

ACKNOWLEDGEMENTS

I am grateful to my advisor, Dr. Michael "Mick" Peterson, for providing me with the opportunity to pursue my Master's degree at UMaine. I would like to thank him for all his time, encouragement and guidance during my graduate study. I wish to thank my thesis committee members, Dr. Donald Grant, Dr. Senthil Vel, and Dr. William Davids for all of their time and assistance with this thesis. I want to thank all the other faculty and staff members in the department and Crosby lab who have given me help during my graduate study at UMaine.

I wish to thank Anthony, Amala, Lin and Jeremy for helping me with my thesis and experimental work. Also thanks to Art for helping me with things around Crosby lab.

Finally, I would like to thank my wife, Rency and my family for their support and care, without which this thesis wouldn't have been possible. I also extend my thanks to all my friends for their encouragement and assistance.

TABLE OF CONTENTS

LIST OF TABLES

LIST OF FIGURES

1 INTRODUCTION

In order to evaluate the condition of a composite material, elastic properties are rarely sufficient. In particular, for polymeric material, damping related measurements in the material provides information about the degree of cross-linking and crystallinity of the polymer [Menard, 1999]. For metals, damping may be related to dislocation motion among other characteristics. For composite materials, in general the interphase and the matrix dominate the damping of the material. In particular, for polymer matrix materials, the fibers are typically very low damping, and the matrix creates damping characteristics that are anisotropic to the same degree as the elastic constants. For matrix materials other than polymers, the same may be true depending on the relative damping characteristic of the matrix and the fibers. This thesis considers damping characteristics of polymer matrix composites as well as reinforced carbon-carbon (RCC).

These characteristics represent perhaps the best hope of developing a true index of state or damage tensor for composite materials. For polymer matrix composites the combined damping and elastic properties can be combined with either temperature or pressure to characterize the interatomic potentials in the matrix. This is the closest to a non-destructive measure of strength that is likely. By describing cross linkage and crystallinity this measure also provides insight into many of the most important degradation mechanisms. While a number of failure mechanisms are important in polymer matrix composites including oxidation and thermal degradation, oxidation processes generally dominate concern in RCC. The most likely result of the oxidation in

RCC, is a significant change in the damping characteristics of the material [Birman and Byrd, 2000]. This is particularly true in materials where matrix properties may differ significantly in the region of the fiber (the interphase). The interphase in some materials is quite distinct, being formed by chemical vapor deposition instead of resin infusion and carbonization. The diffusion of oxygen into the matrix will tend to occur preferentially along paths with reduced density, which also makes sample orientation critical. Various other authors have discussed the importance of damping in evaluating the condition of other high temperature composites including a review article by Birman and Byrd [2000]. In general though, it is important to develop a method that is sensitive to the characteristics of the composite material that are likely to lead to failure. In RCC that characteristic is oxidation. In polymer matrix composites it is likely changes in polymerization or oxidative degradation.

The approach is distinct from a perspective taken too often by the non-destructive testing (NDT) community. In the development of new NDT methods, often a technique is developed by measurement specialists and applied to a wide range of problems to determine where the technique is most effective in finding characteristics of interest. For example, delamination of composite materials and other polymers has been detected by microwave [Summerscales, 1990], shearography [Newman, 1996], ultrasonics [Krautkramer, 1975], laser ultrasonics [Anastasi et al., 1998] and thermography [Zweschper et al., 2003]. As a result, there are a number of methods of finding certain types of defects in composites. Many of these methods continue to be suspect, however because of other influences such as moisture, conductivity of reinforcement and inconsistent matrix properties. Alternatively, if the mechanisms of

failure of a material are investigated, then from that basis a method can be found which is sensitive to the most important failure mechanism. The mechanism should not only exist in a failed part, but ideally should be shown to be a sufficiently early precursor to failure to increase reliability. In RCC identification of the mode is reasonably straightforward, since oxidation of the matrix is the most likely failure mode that is encountered in high temperature applications. It remains however to be shown that any method exists which would have sufficient sensitivity to increased reliability. For other materials, based on environmental conditions, the mechanisms of failure are more variable and would need to be understood in the context of system reliability.

For reliability of structures, distributed cracking is hypothesized as a precursor to failure in the mechanics literature. Thus, the detection of cracks has been a key effort in nondestructive testing. However, even for cracks that are below the critical crack length, the initiation phase represents a significant portion, if not the majority, of the life of the component. Thus, mechanisms associated with crack initiation are of great interest. For composite materials, the initiation failure and initiation phase is typically associated with the matrix of the material. While the process in polymer matrix composites is less straightforward, similar effects may be observed when compared to the material loss mechanisms during oxidation of RCC materials. While the loss of materials in RCC occurs preferentially in the direction of lowest density portions of the matrix, similar diffusion related processes occur in polymer matrix composites that can result in loss of plasticisers or other chemical changes in the matrix. In general, these mechanisms are oxidative or relate to changes in the degree of polymerization. In high strain applications, for elastomeric composites, heat generated by the deformation may

also create regions of localized cross-linking or oxidation. Any of these processes, loss of plasticization, increase in cross-link density, or matrix oxidation will tend to alter the damping characteristics of the matrix. The changes in the damping will occur primarily along the geometric axes where the material properties are dominated by the matrix. However, the geometry of the part can also influence the directions in which the damping changes occur, since part surfaces where a greater percentage of the area is dominated by matrix properties will increase the rate of diffusion. Thus, in general, it is hypothesized that matrix damping may be an effective means of evaluating the condition of composite materials.

In order to understand the damping in these anisotropic materials, verification of the principal material axes in composite samples will first be considered. This measure is required to understand preferred diffusion paths as well as which axis will have high and low damping. After the material axes are determined for a particular specimen, then the damping of the material will be determined in the material principal axes for both dense and oxidized RCC specimens. Similar data for a polymer matrix composite, which is important for marine composites and wood mechanics, is also considered.

This thesis considers this question: The literature suggests that matrix damping of composite materials is an important characteristic for evaluation of the condition of a composite material. Numerous methods exist that allow a damping based "index of state" to be determined for small samples cut from a composite part. However almost without exception these methods are only reactive. This investigation explores the accuracy and repeatability of an ultrasonic method as an absolute measure of material damping. As part of the measurement of damping in an anisotropic material, it is

necessary to ensure that measurements are made along principal material axis. Thus a portion of this work is directed toward ensuring that the sample orientation is optimal. Optimal sample orientation requires recovery of all 21 elastic constants and calculation of the material planes of symmetry. The damping measures are then made in known axes of the material.

1.1 Motivation

Mechanical testing methods present perhaps the most well established methods for obtaining the elastic and damping properties of a material. In addition, mechanical testing is the only practical method of obtaining strength information on materials. The scale of the specimens is dependent on a number of issues associated with the acceptable length scales of materials and edge effects in the sample preparation methods. Using modern three or four point bend fixtures it is possible to obtain visco-elastic properties as well as strength properties for small (less than 60 mm long) beams cut from composite materials. In addition it is possible with mechanical testing to perform the tests at elevated temperatures. For example Kimura and co-workers [1982] found the change in modulus with temperature of a RCC 3mm x 10mm x 60mm long sample using a four point bending specimen. Dynamic mechanical thermal analysis is similarly used in polymer matrix composites. For example, damping was used as a damage variable for water absorption in vinyl-ester glass using 80mm x 13mm x 3mm samples in one study [Fraga et al., 2003]. Young's modulus of a sample was measured from the stress-strain relations recorded from the experiment and compared to another sample evaluated at a higher temperature. While static testing of larger samples in mechanical fixtures is possible, larger specimens create significant cost and complexity even to develop the

basic elastic properties of an anisotropic sample [Bunker, 2002]. In addition, some shear modulus terms are difficult to obtain or are highly uncertain. Non-destructive testing on small samples to obtain the full properties of a composite would be an ideal way of determining the mechanical properties, as well as making it possible to use these measurements in quality control or inspection application.

1.1.1 Effects of Oxidation on RCC

To understand the effects of oxidation on RCC an understanding of the structure of the material is necessary. RCC composites are materials that consist of carbon fibers embedded in a carbonaceous matrix. The particular carbon composite used in this work is composed of a 3-directional, orthogonal, carbon fiber weave. The general configuration is illustrated in Figure 1.1 and Figure 1.2 [Gauthier, 1995]. Figure 1.3 shows an example of the sample used in this thesis

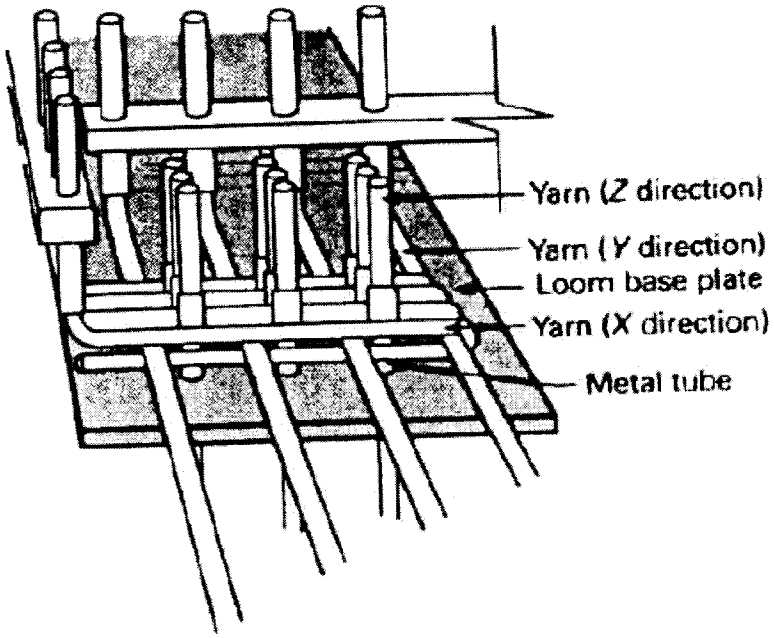

Figure 1.1 3-directional orthogonal weaving [Gauthier, 1995]

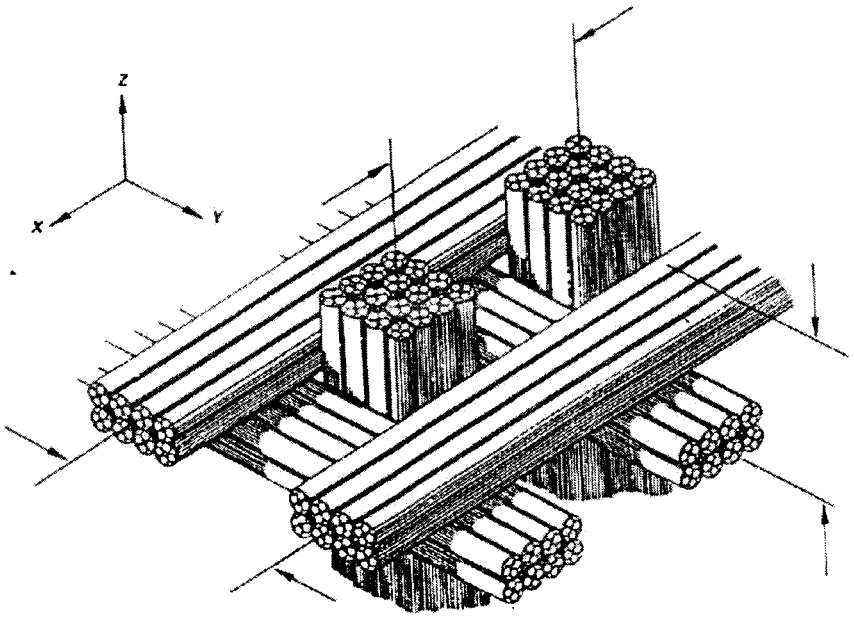

Figure 1.2 3-directional orthogonal weave [Gauthier, 1995]

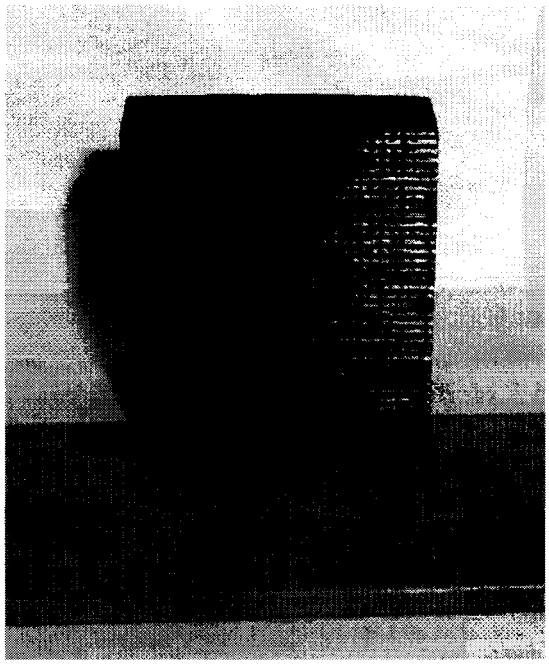

Figure 1.3 Representative RCC sample used in oxidation testing.

RCC is an useful material because of its increased strength at elevated temperatures [Savage, 1993]. One major limitation to the application of RCC composites for high temperatures is the susceptibility to oxidation. Carbon composites readily react with oxygen at temperatures as low as 400°C. This reaction results in loss of material (primarily the matrix) and a degradation of the mechanical properties of the material. Both the strength and the modulus of the material are likely to change as structural material is lost. Consequently, protective coatings are often deposited on the RCC composite in order to prevent this reaction from occurring in high temperature environments. In use these protective coatings can crack and expose the material to an oxidizing environment. This can lead to localized oxidation of the material, which also creates stress concentrations in the part. This is the mechanism, which appears to have led to the loss of the NASA orbiter Columbia [Gehman, et al., 2003].

A continuing need thus exists to perform experiments to better understand the oxidation process and to understand how to measure oxidation in RCC. Currently, no in-situ method exists to study the effects on mechanical properties of oxidation of RCC composites. During oxidation, matrix degradation occurs and thus the damping would be expected to change. Initial results were obtained from a trial run of oxidizing RCC samples. Seven RCC samples were heated to 700°C and were oxidized to different levels (to get different weight loss). Figure 1.4 shows a plot of attenuation vs weight loss.

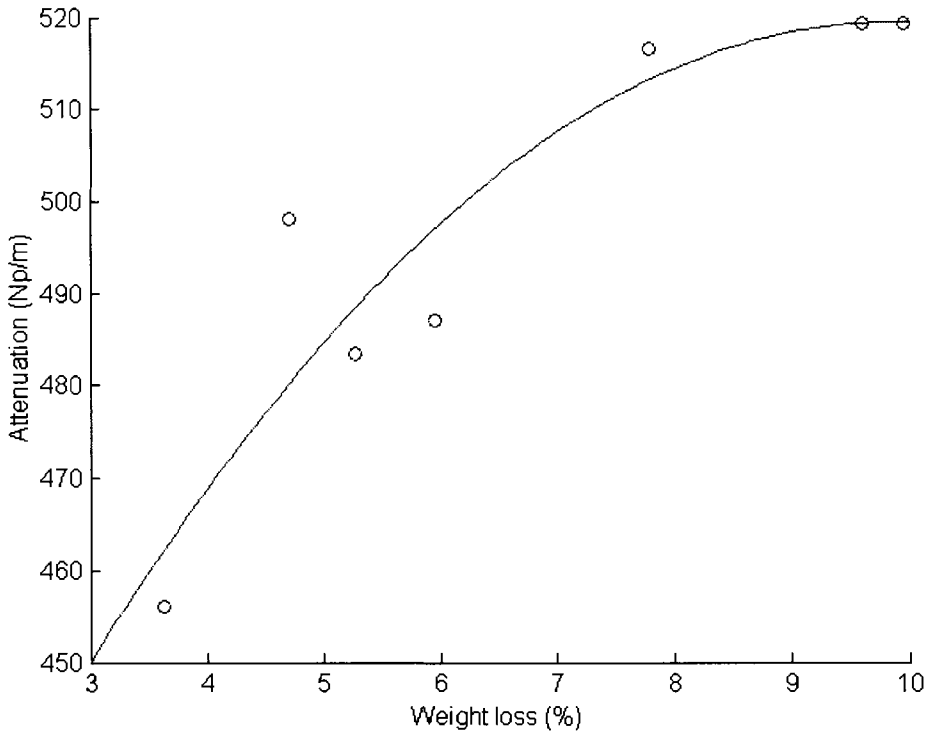

Figure 1.4 Results from the initial runs, effects of oxidation on RCC

In Figure 1.4, a distinct pattern emerges for the behavior of RCC during oxidation. As the weight loss increases the attenuation increases. Most importantly, the changes are quite large at lower weight losses. Other methods are less likely to detect oxidation but show that significant reductions in material strength may occur.

1.1.2 Marine Composites and Tires

Additional applications of the same techniques are possible if sufficient accuracy is obtained. In particular, polymer matrix composites are used extensively and are well suited for marine applications. Inspection is needed to detect manufacturing defects, such as incomplete catalyzation of the resin, or excess catalyst that serves as a plasticizer. Similarly tires are susceptible to heat related changes in the elastomeric

matrix. These changes are most likely to be detected using measurements of material damping. However, like polymeric composites, the changes are expected to be modest. In both systems, layered media needs to be characterized accurately to separate subtle damping changes in a layer. The accuracy and the repeatability of the measurements are critical.

1.1.3 Elastic Properties in an Orthotropic Sample in an Arbitrary Orientation

The first portion of this thesis considers the recovery of elastic properties of a general anisotropic material. Earlier work considered the determination of elastic constants of single crystal materials and RCC using a large number of ultrasonic measurements and optimization [Sun, 2002]. This work was incomplete because of problems with not satisfying constraints in the relationship between the constants. While RCC is nominally orthotropic material with 3 orthogonal planes of symmetry, the manufacturing method suggests that the symmetry may be lower. As such it is assumed that 21 independent variables are required in the constitutive relationship, the most general case of an anisotropic material.

The RCC is not assumed to be orthotropic because of the process used to produce the material. RCC is produced from a 3-dimensional preform, which is nominally orthotropic (3 planes of symmetry). However in RCC, the matrix is introduced into the interstices in the fiber preform using either chemical vapor infusion, resin infusion or a combination of vapor infusion and resin infusion. If resin infusion is used, multiple infusions are used with carbonization of the resin after each infusion. This leads to a diffusion density gradient that may differ in geometry from the matrix preform. Thus while it is tempting to assume that the finished composite retains the

symmetry of the fiber preform, nothing in the material manufacturing process ensures that this is in fact the case. Significant variations of these planes can also exist due to fiber misorientation. The earlier work also considered methods to recover the planes of symmetry from experimental data sets. These data sets are not necessarily oriented in the planes of symmetry and thus may produce a fully populated compliance tensor even in the absence of reduced material symmetry. The ultrasonic technique involved the determination of the compliance tensor in an arbitrary orientation and then defining the orientation. The prior work was effective at implementing the orientation techniques however the optimization algorithms used were suspect because of the instability of the results and not satisfying constraints on compliance explicitly. This thesis extends the optimization procedure and explores methods to improve stability.

1.2 Ultrasonics and Transducers

Ultrasonic waves represent propagating regions of densification and rarefication of an elastic media. By definition ultrasonic waves have frequencies that are too high to be detected by the human ear. While a typical human being can hear sound in the range of 2 Hz to 20 KHz, typical ultrasonic frequencies range from 100 KHz to 80 MHz. In this work 1MHz central frequency transducers are used. This results in a wavelength of approximately 5mm in the material used.

Both generation and detection of ultrasound is typically done using a piezoelectric transducer. The transducer transmits the mechanical energy into the sample. A sketch of an ultrasonic transducer and its components is shown in Figure 1.5

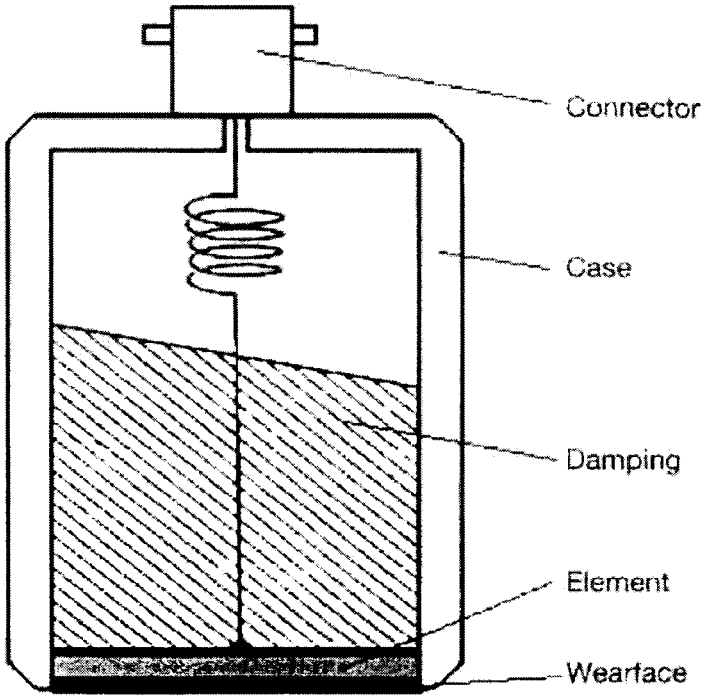

Figure 1.5 A sketch of the components of an ultrasonic transducer [Hellier, 2001]

Three main components of an ultrasonic transducer are the piezoelectric or active element, backing, and an impedance matching plate. The piezoelectric element is capable of both receiving and generating elastic waves, the piezoelectric effect and the inverse piezoelectric effect, respectively. The backing is a highly dense material that controls the propagation of other vibration modes of the transducer by absorbing the energy radiating from the back face of the active element and thus shaping the pulse.

Depending on the way the element of the transducer is cut, either shear or longitudinal waves can be generated. For transmission of the signal into water, shear transducers are not used since the shear wave cannot propagate in liquid medium. However, both shear and longitudinal transducers are used in contact applications where the wave is directly transmitted into a solid material without an intermediate fluid

coupling. Immersion transducers are used in most of the experimental work in this thesis because of the ability to continuously change the angle of the incident wave onto the sample. The range of incident angle is also used to generate both longitudinal and shear waves in the sample as a result of mode conversion at the water interface [Achenbach, 1984]. This provides the large number of signals required to perform the over constrained optimization used to recover the elastic constants.

2 LITERATURE REVIEW

2.1 Methods for Determination of Elastic and Visco-elastic Constants

A number of methods are used to measure the elastic and viscoelastic constants of materials. These are based on either the static or dynamic response of the material to an applied excitation [Schreiber et al., 1973]. The most common method for the determination of the elastic constants was static testing, such as tensile, compressive, and torsional tests [Every and Saches, 1990]. Most of the methods are quite straightforward when applied to homogeneous isotropic solids. For an isotropic material only two independent constants exist. So a simple tensile test can be combined with a torsion test to obtain the elastic constants. Dynamic or creep tests are then used to obtain material damping. Damping measurements must be performed at a range of frequencies since material damping is in general, frequency dependent. Absolute measurement of material damping is challenging because of the dependence on boundary conditions.

In anisotropic materials that are characterized by additional independent elastic constants, mechanical testing is more difficult. In anisotropic materials a number of samples cut at different orientations must be measured. These samples must be representative of the material even though they are cut from different locations. As a result of the testing needs, dynamic methods have been developed. The dynamic methods include ultrasonic transmission [Chimenti, 1997] and resonance method [Migliori and Sarrao, 1997]. Dynamic methods also allow viscoelastic properties to be obtained and can be used to probe some material non-linearities. Most importantly,

dynamic methods can recover all of the elastic constants from a single sample, which reduces the uncertainty in the results. The most widely used methods are, or have been adapted from [Hellwege, 1979]

- Bulk acoustic and ultrasonic wave techniques, including the ultrasonic wave transmission and pulse superposition methods.
- Resonance samples in the shape of rods, bars, parallelepipeds, plates, and more recently spheres.
- Static deformation.
- Light, neutron, and X-ray scattering, including Brillouin Scattering.

In general, the accuracy of the methods differs widely with the list above. The technique of ultrasonic transmission and Brillouin scattering are the most commonly used methods. Brillouin scattering allows the measurements to be made on samples that are a few millimeters in size. Brillouin scattering cannot provide information about the effect of temperature on the elastic constants. In general, ultrasonic transmission methods hold significant advantages if a full set of elastic constants is required [Hellwege, 1979].

2.1.1 Mechanical Tests for Determining Modulus of Anisotropic Materials

During the 1980's, a number of mechanical test methods were introduced along with the development of new composite materials. The development of many new composite materials led to these innovations. Some of the new composite materials included those incorporating toughened epoxy, bismaleimide, polyamide, and high temperature thermoplastic matrix materials, pitch-precursor carbon fibers, and polyethylene and other organic fibers. The new test methods provided a means of

discriminating between the new material systems becoming available. The most common mechanical test configurations were tensile, compressive, shear and flexure. All of these testing methods can be used to obtain both elastic constants and to measure the ultimate strength of the material [Jenkins, 1998].

ASTM D 3039, ASTM D 5467 and ASTM D 2344 illustrate some of the most commonly used tensile, compressive and shear tests for composites [Jenkins, 1998]. All of these tests follow the general rule, apply load, measure strain and find modulus as a ratio of stress over strain. These tests are very specific on how the sample is prepared and on the procedure itself. For characterizing a composite, or any other kind of anisotropic material, these tests require samples to prepared for each orientation. This makes the sample preparation cumbersome. Another major drawback of these tests is the testing environment. The testing environment can affect the repeatability and accuracy of the results [Menard, 1999]. Most of the standard tests are for large samples, i.e., samples whose lengths vary from 5 cm to meters long and width anywhere between 1 cm to meters wide. Most of these tests are conducted at the ambient condition of the lab where the test is being conducted, since controlling of the test condition is very difficult with large samples.

A solution to controlled testing is dynamic mechanical thermal analysis (DMTA), also referred to as dynamic mechanical analysis (DMA). DMA is an experimental technique which analyzes the material's response to an applied dynamic excitation under controlled conditions [Menard, 1999]. DMA achieves this by analyzing small samples. Samples generally are not longer than 4 cm and not more than 5 mm thick. DMA is a widely accepted research technique in the polymer industry for the

determination of material's properties such as viscosity, modulus and damping, providing important information about curing of thermoset resins and the aging of thermoplastics [Menard, 1999]. Even though DMA solves the problem of controlled testing, the number of samples required to characterize a composite is still large.

2.1.2 Ultrasonic Measurement of Material Properties and Optimization

The technique of using ultrasonic transmission to characterize material properties has developed significantly over the past fifteen to twenty years [Chimenti, 1997]. There are many references focusing on methods for obtaining the elastic constants using the ultrasonic technique [Jenkins, 1998]. Chimenti [1997] provides an overall review of the various methods available. In ultrasonic transmission approaches, the specimen is either immersed in a fluid or in direct contact with the transducer. A limitation of the direct contact technique is that it usually requires a fairly thick sample (3 to 5 cm), and it also requires cutting the testing sample at different angles as in mechanical methods [Rokhlin and Wang, 1992; Baudouin and Hosten, 1997]. In the past, one important drawback of the immersion technique, especially for in-service inspections, was the need to immerse the material in a liquid, usually water or oil. However, modern transducer technology has allowed significant reduction in signal noise and air-coupled ultrasonics is now successfully applied for the viscoelastic characterization of composite materials [Hosten, 1991]. Many studies have shown that immersion methods are more straightforward to apply and usually give better results [Papadakis et al., 1991; Hosten, 1991]. Another major advantage over the mechanical testing methods is the reduction in number of samples required to characterize a material. Using one single sample a material can be characterized completely. However, significant complexity is

introduced due to the need to perform constrained optimization to measure the sample [Aristegui and Baste, 1997].

Identification of elastic constants from the measurement of wave velocity using ultrasonic techniques involves evaluating Christoffel's equation [Aristegui and Baste, 1997]. Two major approaches have been applied to find the solution of the Christoffel's equation, numerical techniques [Aristegui and Baste., 1997; Chu et al., 1994] and direct solution expressed in a closed form [Rokhlin and Wang, 1992]. A numerical technique, non-linear optimization, is used in this thesis.

The elastic constants can be reconstructed from the amplitude and velocity data by performing a Newton-Raphson nonlinear optimization to the experimental data. Christoffel's equation is the pivotal equation to be solved to get the required numbers [Aristegui and Baste, 1997]. Christoffel's equation is a cubic equation and applies to plane waves in both isotropic and anisotropic media. The optimization to be performed here is a constrained optimization since the compliance must be positive definite. The format of constrained optimization requires the function to be compared to some limiting value that is established by the constraints [Venkataraman, 2002]. In a constrained optimization problem meeting the constraints is more paramount than optimization. All the numerical techniques used for solving the Christoffel's equation follow the above stated basic rules [Aristegui and Baste, 1997; Chu et al., 1994]. In general velocity data obtained from ultrasonic techniques is subjected to a nonlinear least squared optimization with inequality constraints. Detailed explanation of Christoffel's equation and mathematical derivation to get the stiffness tensor from the Christoffel's equation is included in chapters 3 and 5.

2.2 Polymer Properties and Characteristics: Glass Transition Temperature (Tg)

In order to apply these damping measures to understand the degradation of polymer matrix composites it is helpful to review some basic polymer material properties. The glass transition (Tg) is probably the most fundamental characteristic of a polymer. Among the thermal transitions and relaxations observed in amorphous polymers it is certainly the most important. When an amorphous polymer undergoes the glass transition, almost all of its properties that relate to its processing and/or performance change dramatically. The coefficient of thermal expansion increases from its value for the glassy polymer to a much larger value for the rubbery polymer when the temperature increases to above the Tg. During the transition mechanical properties undergo significant changes as well, the viscosity above Tg is lower than the viscosity below Tg by many orders of magnitude [Bicerano, 1993]. The mechanical experiments clearly demonstrate that the transition from the glassy to the liquid state is purely kinetical phenomenon. Whether the compliance of a sample is small as in a glass, or large as for a rubber, it depends only on the measuring time or the applied frequency. Rubber elasticity originates from the activity of 'α-modes', a major group of relaxation processes in polymer fluids [Strobl, 1996].

The glass transition plays an important role in determining the physical properties of semi-crystalline polymers, whose amorphous portions "melt" or "soften" at Tg while the crystalline portions remain "solid" up to the melting temperature (Tm). A semi-crystalline polymer can be treated as a solid below Tg, as a composite consisting of solid and rubbery phases of the same chemical composition between Tg and Tm, and as a fluid above Tm. The effect of glass transition on physical properties of semi-

crystalline polymers decreases with increasing crystallinity [Bicerano, 1993]. In the context of this thesis the thermal transitions are important because it is widely used in various polymeric systems to describe the degree of crystallinity and cross-link density in a material. In the vicinity of Tg, the modulus typically varies from the glassy modulus (ca. 10^9 Pa) to the rubbery modulus (ca. 10^6 Pa). The general interpretation for the glass transition is "freezing of molecular motions", i.e. competition between the molecular relaxation time scale and experimental time scale.

3 THEORETICAL BACKGROUND

The measurement of elastic properties using ultrasonic waves is dependent on the relationship between modulus and ultrasonic wave velocity. These concepts are important in understanding the results of the measured wave speed. In addition, the reaction between symmetry planes and elastic constants is an important aspect of these measures in anisotropic materials. Finally the relation between the measures of ultrasonic wave attenuation and damping are discussed.

3.1 Equations of General Anisotropic Elasticity

For this application the infinitesimal strain tensor, ε_{ij}, describes the deformation in an acoustical excitation of a body. The strain is related to the particle displacement field u_{kl} through the stress-displacement equation [Fung, 2001]

$$\varepsilon_{ij} = \frac{1}{2}(u_{i,j} + u_{j,i}) \qquad i, j = 1, 2, 3 \tag{3.1}$$

where $u_{i,j}$ and $u_{j,i}$ are the first partial derivative of displacement with respect to the coordinate index j and i, respectively. In the following discussion a summation convention will be observed.

From dynamics, the elastic restoring forces are defined in terms of stress field σ_{ij}. The equation of motion in a freely vibrating body is [Fung, 2001]

$$\sigma_{ij,j} = \rho \ddot{u}_i \tag{3.2}$$

where $\sigma_{ij,j}$ is the partial derivative of stress with respect to the coordinate index j. The superposed double dots, $\ddot{u}_i$ indicates the second partial derivative of displacement with respect to time.

The constitutive equation, Hooke's law, states that the stress is linearly proportional to strain as well as the converse [Auld, 1990].

$$\sigma_{ij} = C_{ijkl}\varepsilon_{kl} \tag{3.3}$$

The elements of the tensor C_{ijkl} in equation 3.3 are called elastic constants.

Since there are nine equations in equation 3.3 (corresponding to all combinations of the subscripts ij) and each contains nine strain terms, C_{ijkl} has indeed a total of 81 components. However, they all are not independent. The symmetry properties of the stress and strain

$$\sigma_{ij} = \sigma_{ji}, \varepsilon_{kl} = \varepsilon_{lk} \tag{3.4}$$

indicate

$$C_{ijkl} = C_{jikl} = C_{ijlk} = C_{jilk} \tag{3.5}$$

Thus, the independent components of C_{ijkl} are reduced from 81 to 36. If Poynting's theorem is applied, it can be shown that

$$C_{ijkl} = C_{klij} \tag{3.6}$$

The number of independent constants are then further reduced to 21. This is the maximum number of independent elastic constants for any material symmetry. If the symmetry properties imposed by the microscopic nature of the material are considered,

the number is typically less than 21. The number of independent constants has range from 2 (isotropic) to 21 (triclinic).

The four subscripts of C_{ijkl} can be simplified to two subscripts by using the following abbreviated subscript notation [Fung, 2001]:

$$\begin{array}{ll} 1 & 11 \\ 2 & 22 \\ 3 & 33 \\ 4 & 23 \textit{ or } 32 \\ 5 & 13 \textit{ or } 31 \\ 6 & 12 \textit{ or } 21 \end{array} \qquad 3.7$$

It can be shown that formally this relates a 3 dimensional 4^{th} order tensor to a 6 dimensional 2^{nd} order tensor if proper normalization is used [Norris, 1988].

The compliance tensor C is written as a 6×6 symmetric matrix form

$$\begin{bmatrix} C_{11} & C_{12} & C_{13} & C_{14} & C_{15} & C_{16} \\ & C_{22} & C_{23} & C_{24} & C_{25} & C_{26} \\ & & C_{33} & C_{34} & C_{35} & C_{36} \\ & & & C_{44} & C_{45} & C_{46} \\ & \textit{sym.} & & & C_{55} & C_{56} \\ & & & & & C_{66} \end{bmatrix} \qquad 3.8$$

or in tensor notation as

$$\sigma_p = C_{pq}\varepsilon_q \qquad 3.9$$

in this section the normalization will not be used, so matrix terminology is followed.

3.2 Understanding Materials: Symmetry Classes

Using the framework of compliance, symmetry of anisotropic materials can be described. In three dimensions, the 32 symmetric point groups can be subdivided into 14 space lattices. These lattices are further grouped into seven crystal systems: triclinic, monoclinic, orthorhombic, tetragonal, cubic, trigonal, and hexagonal [Musgrave, 1970]. The first three symmetry classes (triclinic, monoclinic, and orthorhombic) are considered to be the lower symmetry systems than elastic bodies typically exhibit. The remaining are considered to be the higher systems [Fedorov, 1986]. The derivation of the symmetry groups can be found in various textbooks. Figure 3.1 describes the relation between the axes and the angles of the unit cells in an anisotropic media. Some lower symmetry systems are given here to show how the symmetry properties reduce the number of independent elastic constants.

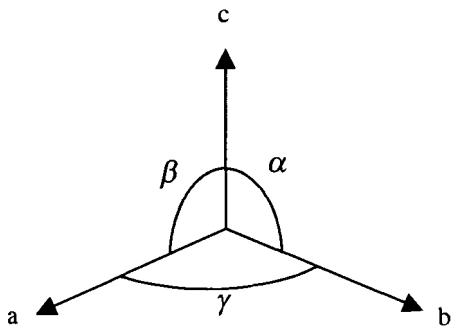

Figure 3.1 Relation between axes and angles in conventional unit cell

3.2.1 Triclinic

Triclinic is the absence of any material symmetry in the solid. There are no relationships between the 21 elastic constants, and none are zero. Figure 3.2 (a) shows 3D space lattices in a triclinic crystal and the corresponding symmetry system. The

angles α, β, γ are not equal and none of the angles are equal to 90^0 [Musgrave, 1970]. This result implies that no planes of symmetry exist in this system or any rotational symmetry.

3.2.2 Monoclinic

A monoclinic crystal has a single mirror symmetry plane, a plane containing axis $\vec{a}$ and $\vec{c}$ in Figure 3.2 (b), with a twofold rotational symmetry axis (axis $\vec{b}$) normal to it. Figure 3.2 (b) also shows that the angles $\alpha=\gamma=90^0$ and $\beta\neq90^0$. The form of the elastic constant matrix for a monoclinic crystal is

$$\begin{bmatrix} C_{11} & C_{12} & C_{13} & 0 & C_{15} & 0 \\ & C_{22} & C_{23} & 0 & C_{25} & 0 \\ & & C_{33} & 0 & C_{35} & 0 \\ & & & C_{44} & 0 & C_{46} \\ & sym. & & & C_{55} & 0 \\ & & & & & C_{66} \end{bmatrix} \qquad 3.10$$

$C_{15} = C_{25} = C_{35} = C_{46} = 0$, and $C_{16}, C_{26}, C_{36}, C_{45}$ are non-zero for a monoclinic material, oriented in the axes of the normal to the symmetry plane.

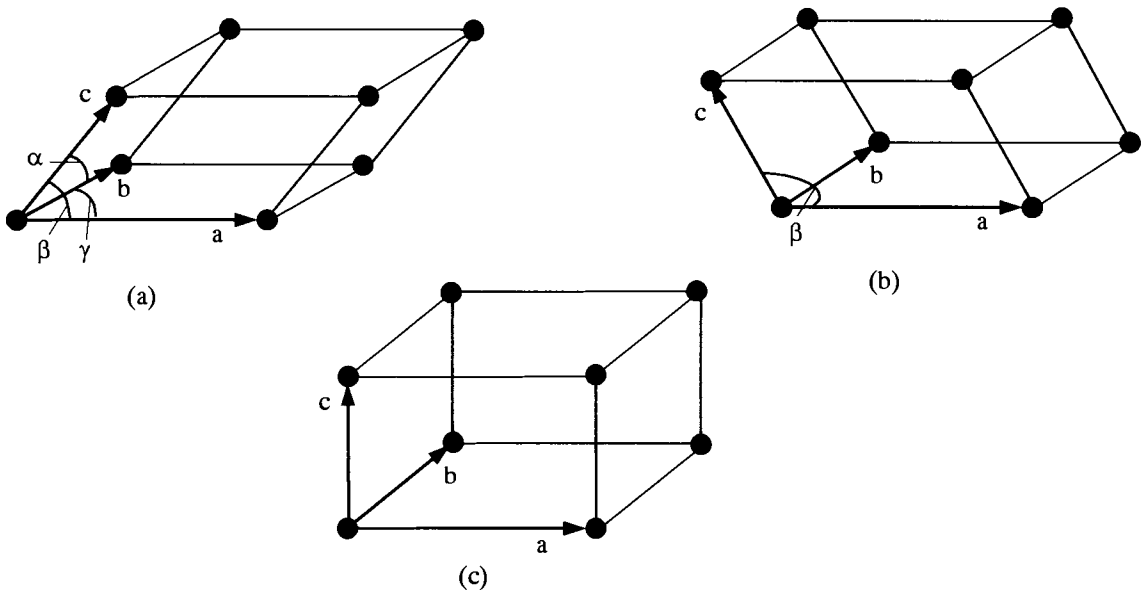

Figure 3.2 An illustration of 3D space lattices and some crystal symmetry systems. (a) triclinic ($\alpha\neq\beta\neq\gamma\neq90^0$); (b) monoclinic (primitive, $\alpha=\gamma=90^0$, $\beta\neq90^0$); (c) orthorhombic ($\alpha=\beta=\gamma=90^0$).

3.2.3 Orthotropic

Orthotropic, also called orthorhombic symmetry, is characterized by three mutually perpendicular mirror symmetry planes and twofold rotational symmetry axes perpendicular to these planes with angles $\alpha=\gamma=\beta=90^0$ as shown in Figure 3.2(c). Orthorhombic materials have nine independent elastic constants. The elastic constants for an orthotropic sample which is oriented with the principal axis forming basis for the coordinates.

$$\begin{bmatrix} C_{11} & C_{12} & C_{13} & 0 & 0 & 0 \\ & C_{22} & C_{23} & 0 & 0 & 0 \\ & & C_{33} & 0 & 0 & 0 \\ & & & C_{44} & 0 & 0 \\ & sym. & & & C_{55} & 0 \\ & & & & & C_{66} \end{bmatrix} \quad 3.11$$

Using these three cases it is then possible to discuss the propagation of elastic waves in anisotropic solids.

3.3 Waves in Anisotropic Solids

From the constitutive equation 3.3 and equations 3.1 and 3.2 we get [Auld, 1990] A plane wave solution to this second order differential equation is assumed to be of the form [Auld, 1990]

$$C_{ijkl} u_{k,jl} = \rho \ddot{u}_i \quad 3.12$$

$$u_k = A_k p_k e^{i(kx-\omega t)} \quad 3.13$$

where A_k are components of the displacement amplitude; p_k are unit displacement polarization vectors traveling in the directions determined by the relationship between the incident angles and the material symmetry axes; $k = \omega/c$ is the wave number with wave speed in the solid c and frequency ω [Auld, 1990]. In general the wave speed c is a function of the elastic compliance of the material and the density of the material. Substituting equation 3.13 into equation 3.12 gives an eigenvalue equation (Christoffel's Equation), then,

$$(C_{ijkl} n_j n_l - \delta_{ik} \rho V^2) p_k = 0 \quad 3.14$$

This is a cubic polynomial in ρV^2, where V is the phase velocity of the ultrasonic wave, δ_{ik} is the Kronecker delta symbol, n is a unit vector in the direction of wave propagation with components of n_1, n_2, n_3. Equation 3.14 can be rewritten in matrix form [Auld, 1990]:

$$\begin{bmatrix} \Gamma_{11} - \rho V^2 & \Gamma_{12} & \Gamma_{13} \\ & \Gamma_{22} - \rho V^2 & \Gamma_{23} \\ sym. & & \Gamma_{33} - \rho V^2 \end{bmatrix} \begin{Bmatrix} p_1 \\ p_2 \\ p_3 \end{Bmatrix} = 0 \qquad 3.15$$

where

$$\Gamma_{ik} = C_{ijkl} n_l n_j \qquad 3.16$$

is referred to as the Christoffel's tensor.

Christoffel's tensor is indeed a second order tensor, subject to the symmetry condition $\Gamma_{ik}=\Gamma_{ki}$ [Hearmon, 1961]. Therefore, six independent components of the Christoffel's tensor exist. Expansion of equation 3.16 following indicial rule gives

$$\begin{aligned}
\Gamma_{11} &= n_1^2 C_{11} + n_2^2 C_{66} + n_3^2 C_{55} + 2n_2 n_3 C_{56} + 2n_3 n_1 C_{15} + 2n_1 n_2 C_{16} \\
\Gamma_{22} &= n_1^2 C_{66} + n_2^2 C_{22} + n_3^2 C_{44} + 2n_2 n_3 C_{24} + 2n_3 n_1 C_{46} + 2n_1 n_2 C_{26} \\
\Gamma_{33} &= n_1^2 C_{55} + n_2^2 C_{44} + n_3^2 C_{33} + 2n_2 n_3 C_{34} + 2n_3 n_1 C_{35} + 2n_1 n_2 C_{45} \\
\Gamma_{12} &= n_1^2 C_{16} + n_2^2 C_{26} + n_3^2 C_{45} + n_2 n_3 (C_{25} + C_{46}) + n_3 n_1 (C_{14} + C_{56}) + n_1 n_2 (C_{12} + C_{66}) \\
\Gamma_{13} &= n_1^2 C_{15} + n_2^2 C_{46} + n_3^2 C_{35} + n_2 n_3 (C_{36} + C_{45}) + n_3 n_1 (C_{13} + C_{55}) + n_1 n_2 (C_{14} + C_{56}) \\
\Gamma_{23} &= n_1^2 C_{56} + n_2^2 C_{24} + n_3^2 C_{34} + n_2 n_3 (C_{44} + C_{23}) + n_3 n_1 (C_{36} + C_{45}) + n_1 n_2 (C_{25} + C_{46})
\end{aligned} \qquad 3.17$$

In order to have a nontrivial solution of the Chirstoffel's equation, the determinant of the coefficient matrix of equation 3.15 must vanish.

$$\left| \Gamma_{ij} - \delta_{ij} \rho V^2 \right| = 0 \qquad 3.18$$

Since the Christoffel's tensor Γ_{ik} is symmetric, its eigenvalues ρV^2 are real and the eigenvectors p_k are mutually orthogonal. Therefore, for any given direction **n**, three modes can be generated with different velocities and polarizations. For the principal propagation directions, pure propagation modes can be generated: one longitudinal wave when P=**n**, and two transverse waves when P×**n**=0. In general, a quasi-longitudinal wave (QL) and two quasi-transverse waves (QT1 and QT2) are excited. The phase velocities corresponding to each of these wave modes are known to be functions of the elastic properties of the material.

3.3.1 Wave Velocity Measurement using Immersion Technique

In the immersion technique the transducers and the sample are immersed in the water or any other coupling media. Consider a coordinate system $R = (\vec{x}_1, \vec{x}_2, \vec{x}_3)$ where R is set at the center of the sample. Unit base vector $\vec{x}_1$ is normal to the interface, with the other two following the right hand rule. For a fluid coupling of an ultrasonic wave into an anisotropic plate, and for an arbitrary incident angle θ, three modes of the wave are excited. A quasi-longitudinal wave (QL), a slow quasi-transverse wave (QT1) and a fast quasi-transverse wave (QT2) are generated in the solid as illustrated in Figure 3.3. These waves propagate at different phase velocities and all the velocity vectors lie in the incident plane. If this plane coincides with a plane of the material symmetry, only one transverse wave and one longitudinal wave are generated [Auld, 1990]. The second transverse polarization is not required to satisfy the boundary conditions at the fluid solid interface.

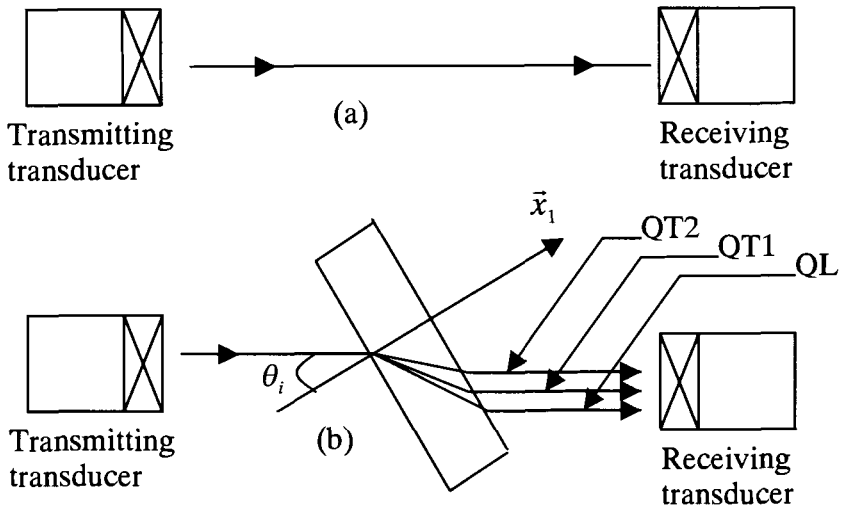

Figure 3.3 Ultrasonic wave velocity measurement (a) through reference media (b) through anisotropic sample [Auld, 1990]

To measure the phase velocity, the length of the wave path through the plate must be known. The relative time delay τ_i between the transmitted signal through the sample and the time through a known media must also be obtained. In this case the known media is the water path without the sample. The time delay is obtained by cross correlation [Peterson, 1997] and will be explained later in section 5.1. The length of the wave path is obtained by Snell-Descartes law [Auld, 1990]. The velocities then can be calculated by the formula [Hosten, 2001]

$$V_i(x_1,\varphi)=\frac{V_0}{\sqrt{1+\frac{V_0\tau_i}{d}\left(\frac{V_0\tau_i}{d}-2\cos\theta_i\right)}} \qquad 3.19$$

where V_0 is the wave velocity in water, τ_i is the time delay, θ_i is the incident angle, d is the thickness of the sample, and $(\vec{x}_1, \varphi)$ indicates the wave incident plane.

In order to identify the full set of elastic constants of a general anisotropic material, experimental data is collected from four incident planes ($\vec{x}_1$, φ), where $\varphi=0^0$, 45^0, 90^0 and 135^0 are called the azimuthal angles [Aristegui and Baste, 1997].

3.3.2 Relationship Between Stiffness Tensor and Engineering Constants

Engineering constants of an orthotropic material are generalized as Young's moduli, Poisson's ratios and shear moduli, as well as some other behavioral constants [Jones, 1975]. These constants are measured in simple tests, which are illustrated later is section 4.2.2.3. The relationship between longitudinal wave speed, c_l and shear wave speed, c_s, to the engineering constants is given by [Grigoriev and Meilikhov, 1997]

$$\rho\, c_s^{\,2} = \frac{E}{2(1+\sigma)} = G \tag{3.20}$$

$$\rho\, c_l^{\,2} = \tilde{\lambda} + 2G = K + \frac{4}{3}G = \frac{G(4G-E)}{3G-E} \tag{3.21}$$

From speeds in all three directions for a material, E_1, E_2, E_3, G_{12}, G_{13} and G_{23} can be determined from equations 3.20 and 3.21. E_1, E_2 and E_3 are the Young's moduli in 1, 2 and 3 direction respectively, G_{12}, G_{13} and G_{23} are shear moduli in 2-3, 1-3 and 1-2 planes respectively. The components of the compliance matrix can be determined as

$$[S_{ij}]=\begin{bmatrix} \frac{1}{E_1} & \frac{-\upsilon_{21}}{E_2} & \frac{-\upsilon_{31}}{E_3} & 0 & 0 & 0 \\ \frac{-\upsilon_{12}}{E_1} & \frac{1}{E_2} & \frac{-\upsilon_{32}}{E_3} & 0 & 0 & 0 \\ \frac{-\upsilon_{13}}{E_1} & \frac{-\upsilon_{23}}{E_2} & \frac{1}{E_3} & 0 & 0 & 0 \\ 0 & 0 & 0 & \frac{1}{G_{23}} & 0 & 0 \\ 0 & 0 & 0 & 0 & \frac{1}{G_{13}} & 0 \\ 0 & 0 & 0 & 0 & 0 & \frac{1}{G_{12}} \end{bmatrix} \qquad 3.22$$

where υ_{ij} is the Poisson's ratio for transverse strain in the j direction when stressed in the i direction. Since stiffness and compliance matrices are mutually inverse, it follows by matrix algebra that their components are related as follows for orthotropic materials

$$C_{11}=\frac{S_{22}S_{33}-S_{23}^2}{S} \qquad C_{12}=\frac{S_{13}S_{23}-S_{12}S_{33}}{S}$$

$$C_{22}=\frac{S_{33}S_{11}-S_{13}^2}{S} \qquad C_{13}=\frac{S_{12}S_{23}-S_{13}S_{22}}{S}$$

$$C_{33}=\frac{S_{11}S_{22}-S_{12}^2}{S} \qquad C_{12}=\frac{S_{12}S_{13}-S_{23}S_{11}}{S} \qquad 3.23$$

$$C_{44}=\frac{1}{S_{44}} \qquad C_{55}=\frac{1}{S_{55}} \qquad C_{66}=\frac{1}{S_{66}}$$

where

$$S=S_{11}S_{22}S_{33}-S_{11}S_{23}^2-S_{22}S_{13}^2-S_{33}S_{12}^2+2S_{12}S_{23}S_{13} \qquad 3.24$$

3.3.3 Determination of Normals to the Symmetry Planes and Principal Coordinate System

Based on the knowledge of the elastic constants C_{ijkl} of an anisotropic material, identification of elastic symmetry possessed by the material was developed by Cowin [1987, 1989] and Norris [1988]. Two tensors, A_{ij} , the Voigt tensor, and B_{ij} ,the dilatational modulus are required to determine the elastic symmetry planes of the material. These tensors are defined as

$$A_{ij} = C_{ijkk}, \quad B_{ij} = C_{ikjk} \tag{3.25}$$

If the abbreviated subscript notation C_{ij} is used and by applying the indicial notation, tensors A and B can be expressed in terms of the components of C_{ij}

$$A = \begin{bmatrix} C_{11}+C_{12}+C_{13} & C_{16}+C_{26}+C_{36} & C_{15}+C_{25}+C_{35} \\ C_{16}+C_{26}+C_{36} & C_{12}+C_{22}+C_{23} & C_{14}+C_{24}+C_{34} \\ C_{15}+C_{25}+C_{35} & C_{14}+C_{24}+C_{34} & C_{13}+C_{23}+C_{33} \end{bmatrix} \tag{3.26}$$

$$B = \begin{bmatrix} C_{11}+C_{55}+C_{66} & C_{16}+C_{26}+C_{45} & C_{15}+C_{46}+C_{35} \\ C_{16}+C_{26}+C_{45} & C_{22}+C_{44}+C_{66} & C_{24}+C_{34}+C_{56} \\ C_{15}+C_{46}+C_{35} & C_{24}+C_{34}+C_{56} & C_{33}+C_{44}+C_{55} \end{bmatrix} \tag{3.27}$$

A vector is normal to a symmetry plane of a linear elastic material, if and only if, the vector is an eigenvector of tensor A and B respectively. These normals are in a specific direction and define a specific axis [Cowin, 1989]. Once the specific directions and specific axes are obtained by solving the eigenvector problem of A and B, the elastic symmetry of the anisotropic material can be determined.

Theoretically, for an orthotropic material, the three eigenvectors of tensor A and B are coincident and are aligned with their crystallographic directions [Cowin Mehrabadi, 1987]. For a monoclinic media, only one pair of eigenvectors is identical.

In the case where none of the eigenvectors are in common indicates that the material tested possesses triclinic symmetry. However when using experimental data, errors in the measurements result in eigenvectors of A and B that do not exactly line up. Since the eigenvectors of A and B are orthogonal eigenvectors, respectively, a normal to the symmetry plane is contained in an angle around the average directions between the closest eigenvectors of A and B [Aristegui and Baste, 2000]. The closest eigenvectors of A and B can be determined by investigating the angular deviation between each pair of eigenvectors. In general the eigenvector pair that exhibits the small angular deviation is considered to be a good estimate of a normal to a symmetry plane [Aristegui and Baste, 2000]

Once the normals to the symmetry planes are known, recovery of the principal coordinate system becomes relevant. In some design applications, knowledge of the principal coordinate system is necessary to predict the misorientation between the symmetry axes and the geometric axes within the material. It can also increase the understanding of the warpage and coupled deformation.

As described in section 3.2, seven symmetrical crystal systems exist. The number of symmetry planes it possesses and the orientations of these symmetry planes characterize each system. The orientation of a principal coordinate system, R^P with respect to an observation coordinate system R as defined in section 3.3.1 can be specified by a set of Euler's angles $\delta = (\alpha, \beta, \gamma)$. Euler's angles relate the two coordinate systems R^P and R through a set of successive rotations between the two systems.

No general agreement on the notation of Euler's angles exists, but one of the most common, viz. α, β, and γ, in sequence, is shown in Figure 3.4. The coordinate

system R with a set of Cartesian axes $\vec{x}_1, \vec{x}_2$ and $\vec{x}_3$ is first rotated through an angle α about the $\vec{x}_3$ axis. A further rotation through angle β about the transformed $\vec{x}_1$ brings the body into a coordinate system R'. Finally a second rotation γ about the transformed $\vec{x}_3$ put the system into a coordinate system R^P with a set of Cartesian axes $\vec{x}_1^P$, $\vec{x}_2^P$, and $\vec{x}_3^P$. The rotations are performed as counterclockwise as one looks to the origin O along the axis of rotation [Shames, 1966]. It is also important to note that the orientation of the rotated coordinate frame is dependent on the order of the rotations.

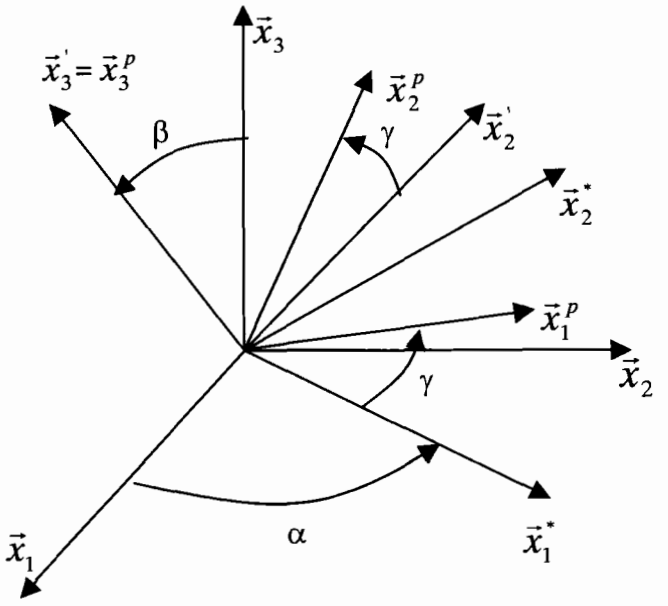

Figure 3.4 Illustration of Euler's angles $\vec{x}^*$ represents the rotated axes

Transformations from the initial R to the coordinate system R^P may also be obtained through three-transformation tensors $a(\alpha)$, $a(\beta)$, $a(\gamma)$.

$$\{\vec{x}_i^{\,P}\} = [a(\alpha)][a(\beta)][a(\gamma)]\{x_i\} = [M]\{\vec{x}_i\} \qquad 3.28$$

where

$$[a(\alpha)] = \begin{bmatrix} \cos(\alpha) & \sin(\alpha) & 0 \\ -\sin(\alpha) & \cos(\alpha) & 0 \\ 0 & 0 & 1 \end{bmatrix}$$

$$[a(\beta)] = \begin{bmatrix} 1 & 0 & 0 \\ 0 & \cos(\beta) & \sin(\beta) \\ 0 & -\sin(\beta) & \cos(\beta) \end{bmatrix} \qquad 3.29$$

$$[a(\gamma)] = \begin{bmatrix} \cos(\gamma) & \sin(\gamma) & 0 \\ -\sin(\gamma) & \cos(\gamma) & 0 \\ 0 & 0 & 1 \end{bmatrix}$$

which can be combined to give

$$[M] = \begin{bmatrix} \cos(\alpha)\cos(\gamma) - \sin(\alpha)\cos(\beta)\sin(\gamma) & \sin(\alpha)\cos(\gamma) + \cos(\alpha)\cos(\beta)\sin(\gamma) & \sin(\beta)\sin(\gamma) \\ -\cos(\alpha)\sin(\gamma) - \sin(\alpha)\cos(\beta)\cos(\gamma) & -\sin(\alpha)\sin(\gamma) + \cos(\alpha)\cos(\beta)\cos(\gamma) & \sin(\beta)\cos(\gamma) \\ \sin(\alpha)\sin(\beta) & -\cos(\alpha)\sin(\beta) & \cos(\beta) \end{bmatrix}$$

3.30

Locating the principal coordinate system R^P (if it exists within the material) is equivalent to the determination of the set of angular unknowns, $\delta=(\alpha, \beta, \gamma)$. Each of the angular unknowns corresponds to a normal to the symmetry plane and transforms the coordinate system from R^P to R. In general, two rotations of the coordinate system are enough to characterize the orientation of the principal coordinate system R^P [Auld, 1990; Aristegui and Baste, 2000]. In other words, any principal coordinate system R^P, with respect to the observation coordinate system R, can be characterized by a set of angular unknowns with at least one of these unknowns being equal to zero. Therefore the transformation matrix [M] in Equation 3.30, if $\gamma=0$ as in this thesis, can be reduced to

$$[M]=\begin{bmatrix} \cos(\alpha) & \sin(\alpha) & 0 \\ -\sin(\alpha)\cos(\beta) & \cos(\alpha)\cos(\beta) & \sin(\beta) \\ \sin(\alpha)\sin(\beta) & -\cos(\alpha)\sin(\beta) & \cos(\beta) \end{bmatrix} \quad 3.31$$

For the case where the material possesses higher symmetries (tetragonal, hexagonal or isotropic), the principal coordinate system can be identified, based on the symmetry model assumed. The orientation of the axes is found by investigating the deviation between the elastic constants reconstructed in R^P and the one satisfying the chosen symmetry model [Aristegui and Baste, 1997]. In the case where the material possesses only a single symmetry plane, identification of the symmetry is reduced to finding one unknown of the Euler's angles with the two other angles zero. On the other hand, if no symmetry can be determined, three Euler angles $\delta=(\alpha, \beta, \gamma)$ are necessary to search for R^P [Aristegui and Baste, 1997].

3.4 Linear Viscoelasticity

In addition to the elastic properties the damping properties are used in this thesis to describe the equations of state of the materials. This explanation can be done in terms of linear viscoelasticity in the principal axis of the material because the elastic properties have been measured and the sample has been oriented in the principal material axes prior to measuring damping. Linear viscoelastic behavior is often idealized as a combination of springs, to represent purely elastic or Hookean behavior, and dashpots to represent purely viscous or Newtonian behavior.

The one-dimensional problem is suitable for samples oriented in principal axes as well as being often used as a tool to help understanding linear viscoelastic behavior. In this case, the combination of elements - spring and dashpot – is arranged in series and

in parallel. The simplest models are the Maxwell model and the Voigt (or Kelvin) model Figure 3.5 [Mase, 1970]. The stress-strain relation for the Maxwell model is [Mase, 1970]:

$$\frac{\dot{\sigma}}{k}+\frac{\sigma}{\eta}=\dot{\varepsilon} \tag{3.32}$$

and for the Voigt model is [Mase, 1970]:

$$\sigma = k\varepsilon+\eta\dot{\varepsilon} \tag{3.33}$$

where k is the spring constant and η is the viscosity constant of the dashpot.

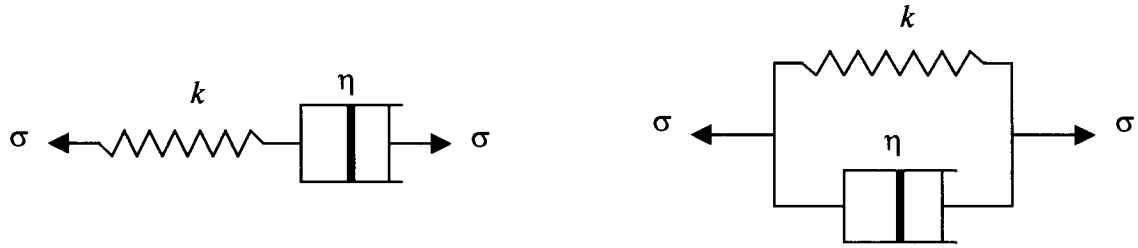

(a) Maxwell Model (b) Voigt Model

Figure 3.5 Simplified one-dimensional viscoelastic models

The simple Maxwell and Voigt models are not adequate to completely represent the behavior of real materials. More complicated models afford a greater flexibility in portraying the response of actual materials. A three parameter viscous model consisting of two dashpots and one spring, and known as the standard linear solid is shown in Figure 3.6 [Mase, 1970].

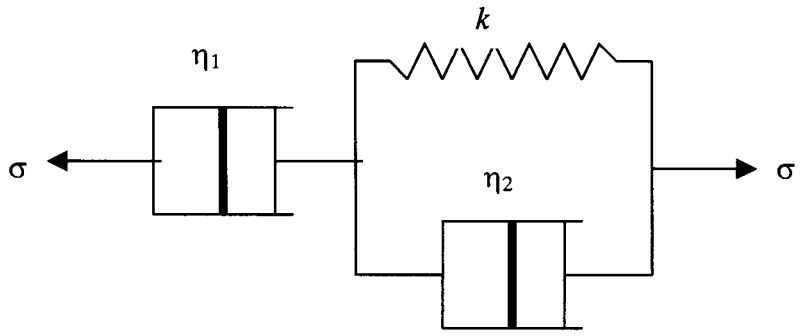

Figure 3.6 Three parameter viscous model

A four parameter model consisting of two springs and two dashpots may be regarded as Maxwell unit in series with a Voigt unit as illustrated in Figure 3.7 [Mase, 1970].

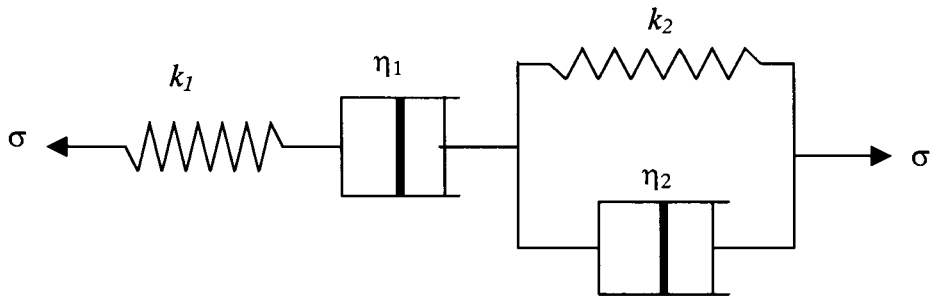

Figure 3.7 Four parameter model

The four parameter model is capable of all three of the basic viscoelastic response patterns. Thus it incorporates "instantaneous elastic response" because of the free spring k_1, "viscous flow" because of the free dashpot η_1, and, "delayed elastic response" from the Voigt unit. The stress strain equation for any of the three or four parameter models is of the general form [Mase, 1970]:

$$p_2\ddot{\sigma} + p_1\dot{\sigma} + p_0\sigma = q_2\ddot{\varepsilon} + q_1\dot{\varepsilon} + q_0\varepsilon \qquad 3.34$$

Where the p_i's and q_i's are coefficients made up of combinations of the k's and η's and depend upon the specific arrangement of the elements in the model [Mase, 1970].

Complex modulus notation is used to mathematically represent the characteristic of a viscoelastic material, by combining damping and stiffness expression [Jenkins, 1998]. Another form of the stress strain equation represented by equation 3.34, using complex modulus notation, is

$$\sigma(t) = C^*(\omega)\,\varepsilon(t) \qquad 3.35$$

where

The complex compliance C^* is

$$C^*(\omega) = E'(\omega) + iE''(\omega) = E'(\omega)\left[1 + i\,\eta\ (\omega)\right] \qquad 3.36$$

and the loss factor η is

$$\eta(\omega) = \frac{E''(\omega)}{E'(\omega)} = \tan\delta\ (\omega) \qquad 3.37$$

ω is the frequency, t the time, $E'(\omega)$ and $E''(\omega)$ are the elastic (or storage) modulus and loss modulus, respectively, and $\delta(\omega)$ is the phase angle between the applied stress and strain. The relationship between these quantities is shown in Figure 3.8 and Figure 3.9. When we apply an oscillating stress to a sample, the response signal will not be similar to the applied signal. This is due to the various losses attributed to the elastic and viscous behavior of the sample, the strain lags the applied stress by the phase angle δ [Menard, 1999].

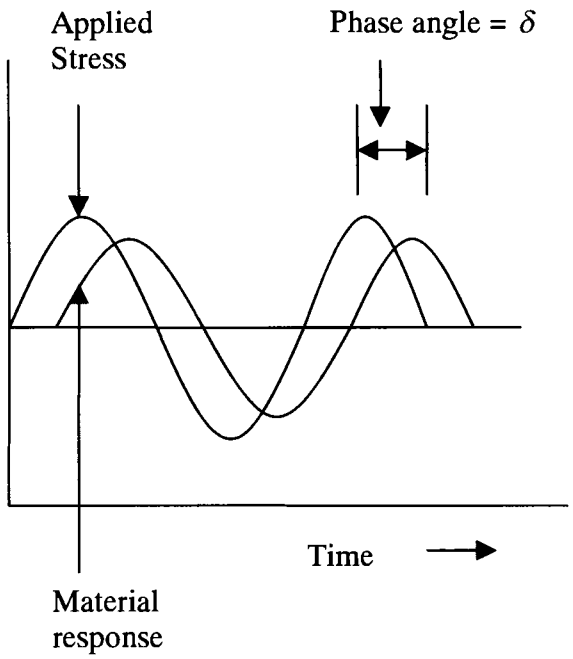

Figure 3.8 Applied stress and response of a sample

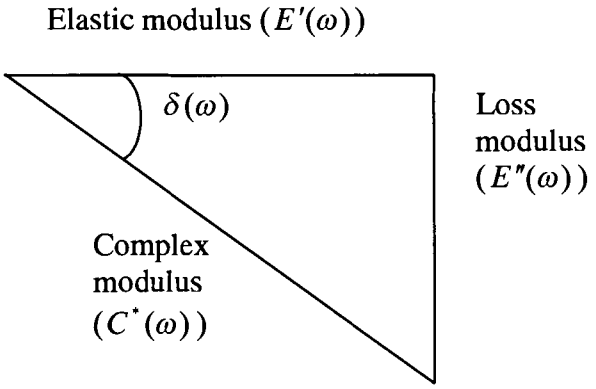

Figure 3.9 Graphical relationship between C^*, E' and E''

The tangent of the phase angle, tan δ, is the ratio of loss modulus to storage modulus and is a valuable indicator of the material's relative damping ability.

In contrast to many introductory texts on linear viscoelasticity the current interest is in the measurement of damping effects on an elastic wave. The phase velocity c, attenuation α and frequency ω of an elastic wave can all be related to this linear viscoelastic behavior [Christensen, 1971]. The Fourier transformed displacement, $\bar{u}(x,\omega)$, has a solution in the form:

$$u(x,t) = B\, e^{-\alpha t} e^{i[kx-\omega t]} \tag{3.38}$$

which is a one dimensional version of the plane wave solution (equation 3.12) with an attenuation term $e^{-\alpha t}$ added to describe losses due to viscous effect:

$$\alpha = \frac{\rho^{1/2}\omega\, E''}{\left|C^*(\omega)\right|} \tag{3.39}$$

ρ is the density of the sample

The longitudinal wave velocity [Grigoriev and Meilikhov, 1997]:

$$c = \sqrt{\frac{G(4G-E)}{\rho(3G-E)}} \tag{3.40}$$

$$E = 2G(1+\upsilon) \tag{3.41}$$

where E is the Young's modulus, G is the shear modulus and υ is the Poisson's ratio

The solution in equation 3.37 represents the propagation of a harmonic wave moving in the positive x direction, c and α are the phase velocity and attenuation, respectively, and the constant B is to be determined from boundary conditions. Through some algebraic reductions, c and α can be written as

$$c = \left(\sqrt{\frac{G(4G - E)}{\rho(3G - E)}} \right) \sec(\delta(\omega)/2) \qquad 3.42$$

$$\alpha = c^{-1}\left[\omega \tan\left(\frac{\delta(\omega)}{2}\right) \right] \qquad 3.43$$

and from equations 3.42 and 3.43 tan δ can be determined

$$\delta(\omega) = 2\left(\tan^{-1}\left(\frac{c\alpha}{\omega} \right) \right) \qquad 3.44$$

determination of the attenuation coefficient is illustrated in section 5.2

4 EXPERIMENTAL SYSTEM

Two separate experimental tests were performed. First, a procedure for obtaining the data required for extracting the elastic modulus and attenuation of composite materials at room temperature. In addition data was collected to study the effects of oxidation on RCC.

4.1 Experimental Setup

4.1.1 Ultrasonic Immersion Setup for Velocity Data Determination

The experimental portion of this work uses a conventional immersion ultrasonic system, as shown schematically in Figure 4.1. Two matched immersion transducers with center frequency of 1.0 MHz (Parametrics, model V 303) are placed on opposite sides of the sample. These are conventional piezo-electric units with one of the transducers used as a transmitting transducer and the other as a receiving transducer.

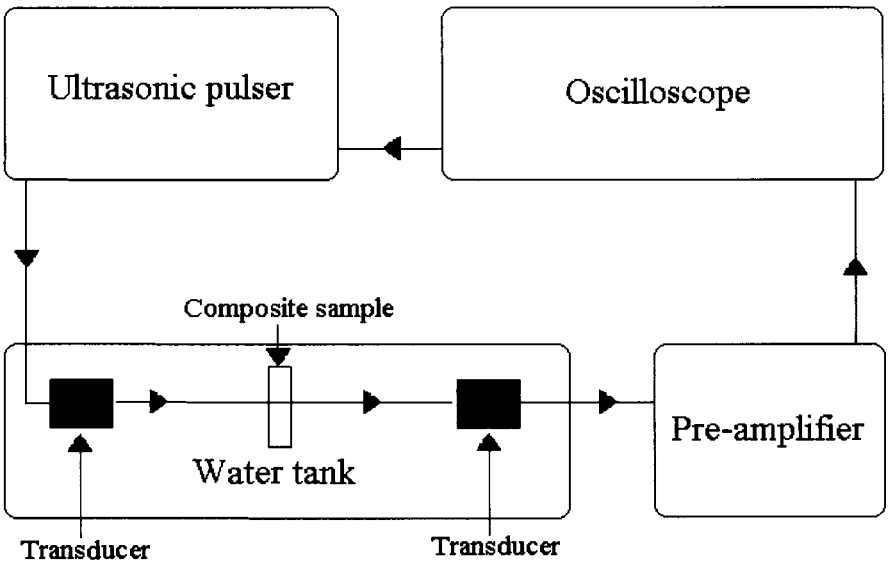

Figure 4.1 Experimental Setup

The position of the transmitting transducer is fixed along the center of the sample i.e. $\vec{x}_1$ is fixed according to the coordinate system defined in section 3.3.1. The position of the receiving transducer is adjusted manually to the peak of the signal in the x_1 and x_2 axes of the sample coordinate system. Alternatively, it is possible to compute the position using Snell's law [Hosten, 1991]. Figure 4.2 is a photograph of the experimental set up.

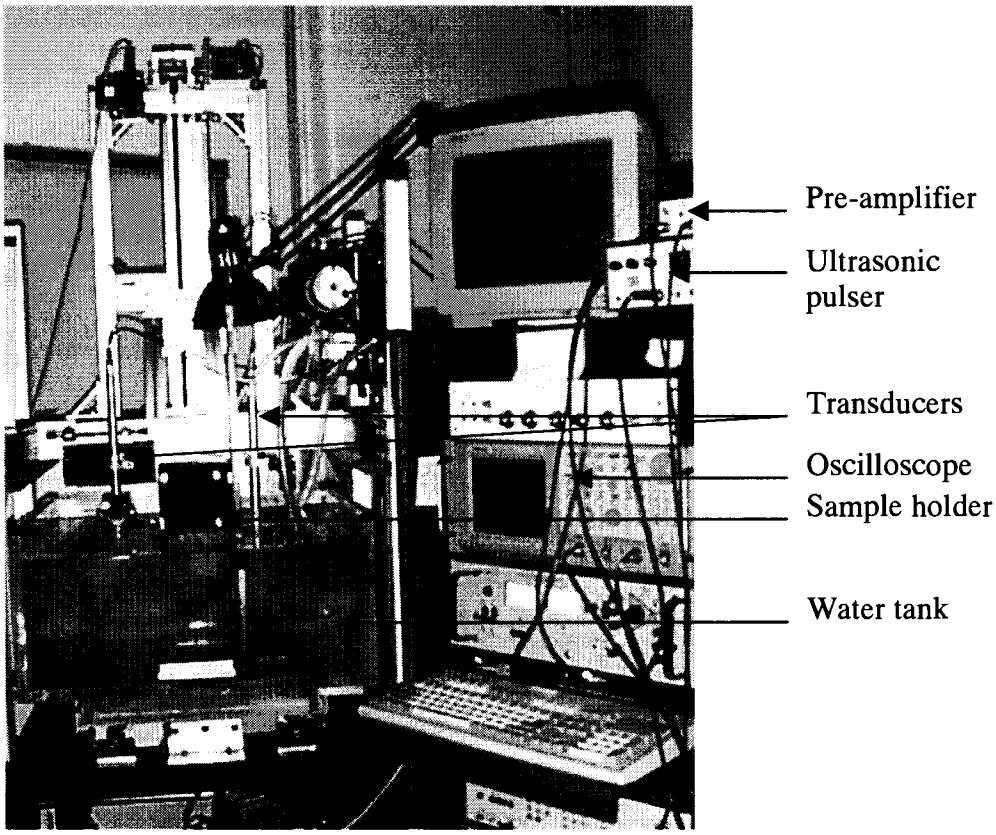

Figure 4.2 Photograph of experimental setup

4.1.2 Pulser, Pre-Amplifier and Oscilloscope

A conventional spike pulser (Panametrics model 5072PR, Waltham, MA) is used to create the energy that is converted to an ultrasonic signal within the piezoelectric material of the transmitting transducer. This pulser has a built in pre-amp. Both the

built in pre-amp and a separate pre-amp are used during the testing. The receiving transducer is connected either to the receiver input on the pulser receiver or to a separate pre-amp (Panametrics 5660C, Waltham, MA). The separate pre-amp is used to improve the signal isolation which is needed due to the low signal to noise ratio. The separate pre-amp used in this work has two gain settings, 34db and 54db. Signals recorded in this work are amplified using the 54db gain.

The amplified received ultrasonic signal is sent to an oscilloscope (Tektronix Model TDS 520A, Beaverton OR). Consistent setting of the oscilloscope time is required for later signal processing. The oscilloscope is used with the following settings, all of which control the time settings of the acquired signal.

0% Trigger position

15000 points per record

250 Megasamples per second

45 μsec time delay

Signal averaging is set at 50 signals to improve the signal to noise. The time delay is dependent on the thickness of the sample. The sampling rate, of 250 Ms/sec, makes it possible to measure time delays within the sample to a precision of 4 nanoseconds. Amplitude settings are adjusted to maximize the vertical resolution of the received signal. In order to obtain the full vertical resolution (8 bits) the signal must fill all 10 vertical segments of the scope only 8 of which are displayed on the screen.

4.1.3 Experimental Setup for Determining the Initial Guess for Stiffness Tensor

Contact transducers are used to obtain the initial guess for the stiffness tensor. Contact transducers cut to generate a longitudinal wave, and contact shear transducers are used to find the time delay in the signal in all three directions. Figure 4.3 and Figure 4.4 shows the experimental setup.

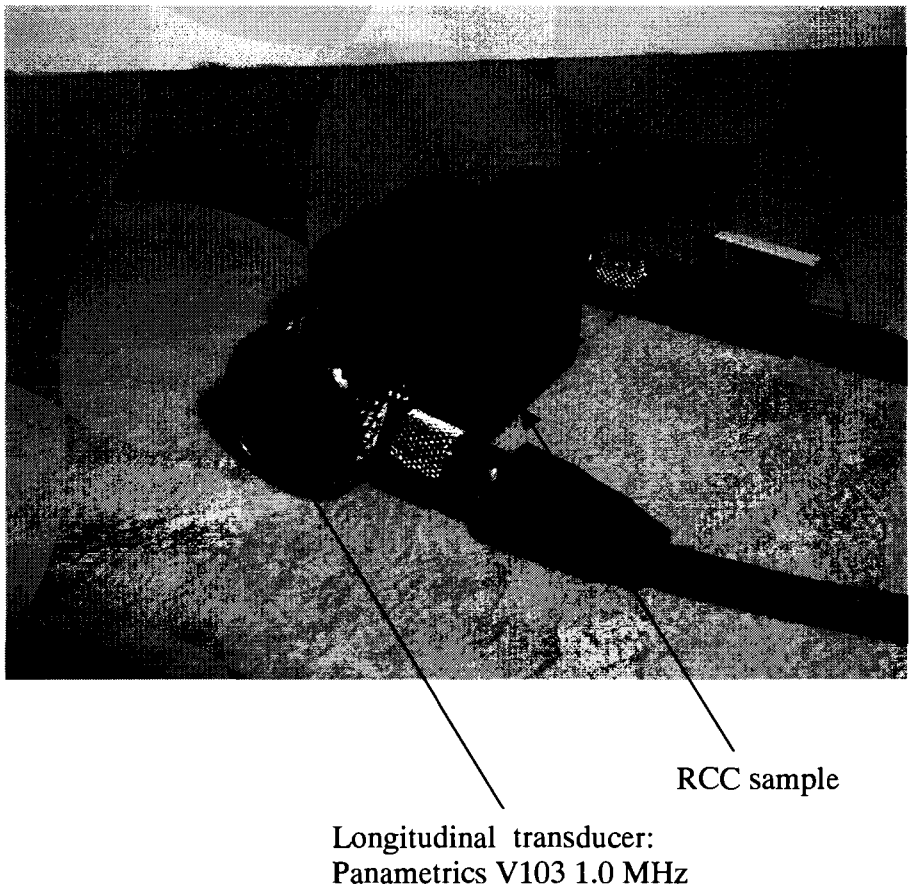

Figure 4.3 Longitudinal contact transducers coupled to the sample

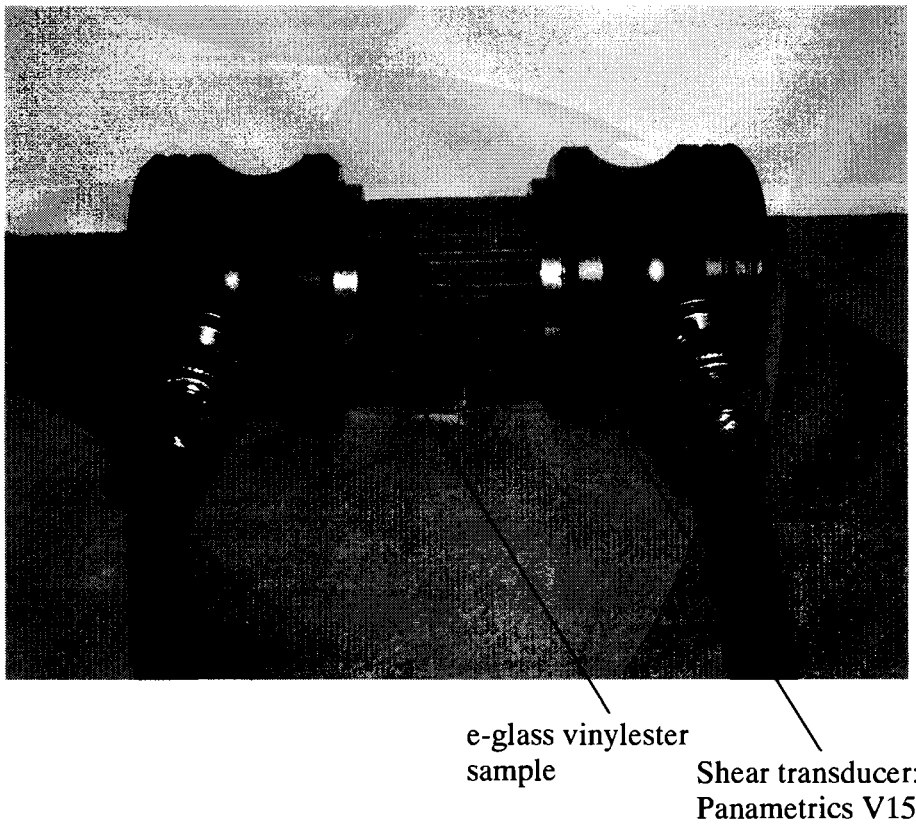

Figure 4.4 Shear contact transducers coupled to the sample

Proper coupling is applied between the transducer and the sample to ensure the good transmission of ultrasonic waves. For longitudinal transducers UT-30 ultrasound couplant (Sonotech Inc) is used as a couplant and petroleum jelly is used as couplant for shear transducers. The transducers are firmly pressed on to the measuring faces of the sample by hand while recording the signal using an oscilloscope. The same procedure is repeated for all the 3 faces using both longitudinal and shear transducers.

4.1.4 Experimental Setup for Determining the Effects of Oxidation on Attenuation

The same samples used to obtain velocity data and attenuation data at room temperature are used to obtain oxidation data. The samples are placed in a tube furnace. The furnace is a conventional tube type, 3-zone furnace (Lindberg Model 55346, Watertown WI) that has three individual embedded alloy heating elements (type LGO), located near the center. The furnace is capable of producing temperatures up to 1100° C. The three heating elements surround a 40mm outer diameter (32mm inner diameter) mullite tube (Anderman Ceramics, model EWF .610, London UK) that runs horizontally through the furnace extending out to the right and left hand sides. Alumina fiber insulation also surrounds the mullite tube through the furnace.

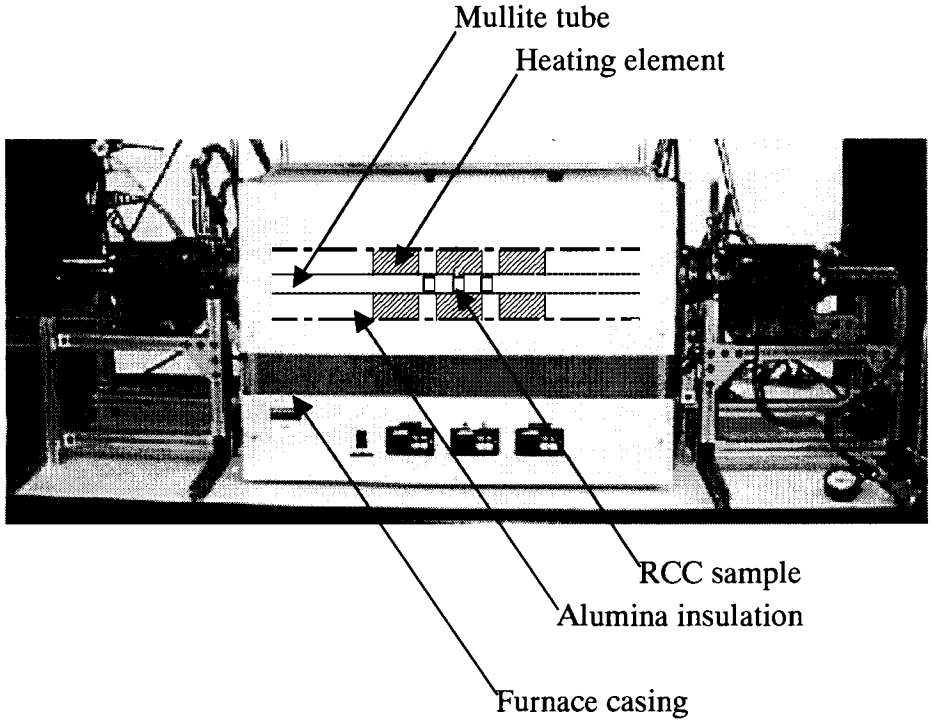

Figure 4.5 Photograph of the furnace with cross sectional details

The mullite tube allows the entire apparatus, shown in Figure 4.5, to be sealed from the outside of the furnace. This allows the RCC composite to be held in a controlled atmosphere furnace. Without the tube extending out of the furnace, sealing the RCC sample inside a high temperature atmosphere is difficult.

4.2 Experimental Preparations and Procedures

Sample preparations and the procedure for the experiment is particularly critical for the RCC because of the sample layup. In the RCC orientation of the sample is critical. Similar samples are used for the polymer matrix composites, however preparation is somewhat less critical.

The original block of RCC obtained through Applied Thermal Sciences (Sanford, ME) was 124 mm x 122 mm x 41 mm ($\cong$ 5 x 5 x 1.5 inches). Specimenss were cut from this original block for a number of experiments. The specimens used in these tests were cut from larger sections using a tile saw (MK diamond products, model MK101, Torrance, CA). The opposing sides of the test specimens are cut as close to parallel as possible in order obtain accurate data. The thickness of each specimen was cut to 9mm. The height and width of the samples were cut to 25mm and 24mm respectively. The thickness dimension is critical for the attenuation measure because of the direct effect as well as changes in measured attenuation due to non-parallel faces. Keeping the overall dimensions of all RCC composite specimens similar simplifies the experiments and calculations. Each sample is marked to identify the orientation with respect to the original block.

All of the specimen dimensions are carefully measured, accurate to 0.01mm, recorded and placed in a small, labeled plastic bag. The bags were labeled with the date

that the sample was tested. Each specimen was weighed, using a tabletop scale (Davis Instruments, model SV-200 Baltimore MD) accurate to 0.01 g. Once these specimens were cut, measured and recorded, they were ready to be tested. e-glass vinylester samples are cut from 460 mm x 30mm x 25mm composite beams to the same dimensions as of the RCC samples.

The experimental procedure consists of two separate parts. First, a procedure for obtaining the data required for extracting the elastic modulus and attenuation of e-glass vinylester and RCC at room temperature. A separate procedure is required to perform the controlled oxidation of the RCC samples.

4.2.1 Elastic Modulus and Attenuation Determination

One of the methods for obtaining velocity data in an ultrasonic immersion technique is to compare the signal through the sample with a signal through the medium without a sample. Measurements are performed with 4 incident planes, azimuthal angles being 0^0, 45^0, 90^0, 135^0 associated at a range of different incident angles. In each of the incident planes, 25 measurements were carried out corresponding to 25 incident angles (0^0 to 24^0). At each incident angle, the relative time delay was measured from the signals received. Only the highest amplitude mode was measured. All the measurements are conducted in a water tank where the temperatures are monitored continuously. A reference signal is also recorded at the same water temperature. The reference signal is obtained by removing the sample and allowing the ultrasonic signal to travel directly from the transmitter to the receiver. Each of the data set consisting of 100 signals is compared with the reference signal to obtain the velocity data. To obtain the attenuation and damping property only one of the data set, the one with azimuthal angle

and incident angle at 0° to the material principal axis is considered. This signal is compared with the reference signal to obtain the attenuation.

4.2.2 Determination of Effects of Oxidation on Attenuation

For the controlled oxidation studies the samples are placed in the furnace and heated to 700° C in an inert environment. Compressed nitrogen is used here. The samples are maintained at 700° C for 45 minutes in an oxidizing environment allowing it to oxidize, for this the nitrogen is disconnected and compressed air is supplied through the furnace. Then the samples are removed and weighed. The oxidized samples are tested in an immersion process as explained in section 4.1.1 for obtaining the attenuation data, ie, azimuthal angle 0^{0} and incident angle 0^{0} (one data set).

4.2.3 Experimental Determination of the Initial Guess Used in Stiffness Matrix Algorithm

The determination of initial guess for the nonlinear optimization algorithm used for recovery of the stiffness matrix is explained in this section. A cube of dimension 0.026 x 0.091 x 0.021 m is cut from the same RCC sample used for the recovery of the tensor. The setup shown in section 4.1.3 is used. The time delay for longitudinal and shear (transverse) waves are determined using the setup. A coordinate system as illustrated in section 3 is followed for obtaining the initial guess. Longitudinal waves transmitted through thickness in 1, 2 and 3 directions yield E_1, E_2 and E_3 respectively. This is explained in detail in section 3.3.2. Time delays are recorded in each of these 3 directions and the longitudinal wave speed is calculated as:

$$c_l = \frac{Thickness\ of\ sample\ in\ direction\ of\ measurement}{time\ delay} \qquad 4.1$$

A similar method is followed with a shear wave transducer. The time delay measured in different directions yield G_{23}, G_{13} and G_{12} respectively. When the shear transducer is placed in the 1 direction both G_{13} and G_{12} can be determined from the time delay measured and the transducers aligned in the 2 direction recovers G_{23}. This is explained in detail in section 3.3.2. In this case, also, the shear wave speed is calculated as:

$$c_s = \frac{Thickness\ of\ sample\ in\ direction\ of\ measurement}{time\ delay} \qquad 4.2$$

For calculation purposes Poisson's ratios, υ_{12}, υ_{13} and υ_{23} is assumed to be 0.3 and the Maxwell-Betti reciprocal theorem is followed. This method is used to obtain the initial guess for the RCC samples only, initial guess for e-glass vinylester is obtained from a reference paper [Peterson, et al., 2002]. The ultrasonic signals obtained using the contact transducers are attenuated more in the case of e-glass vinylester making it difficult to do analysis.

5 SIGNAL PROCESSING

In order to obtain engineering properties from ultrasonic testing, significant signal processing is required. To obtain the time delay required for elastic modulus, very high accuracy is required. The measurement of attenuation requires that the effects of the instrumentation be removed from the measurement. Finally in order to obtain the full compliance tensor from the multiple velocity measurements, a technique is required to extract 21 constants from 100 equations. These techniques are described in the following section.

5.1 Cross-correlation

To obtain accurate relative time delays cross-correlation is used [Peterson, 1997]. Cross-correlation algorithms are used to estimate the time delay difference (τ) between two signals. In this thesis an ultrasonic waveform transmitted through water (the reference signal) is compared to a signal through the RCC sample. Cross correlation techniques have broad applications in radar, digital communications and other areas in science and engineering.

Assume two time domain signals to determine the time delay, $x(n)$ and $y(n)$ are available that are sampled at discrete even time intervals n. The samples are evaluated at discrete intervals and satisfy all discrete time sampling constraints. The cross correlation between these two signals is defined by [Silvia, 1986]

$$r_{xy}(\tau) = \sum_{n=-\infty}^{+\infty} x(n)y(n-\tau) \qquad 5.1$$

where τ is time shift or time delay parameter and the subscript xy indicates the signals used in the cross-correlation. The inner product of two vectors in a finite dimensional domain is [Silvia, 1986]

$$\langle x(n), y(n) \rangle = \sum_{n=0}^{N-1} x(n) y(n) \qquad 5.2$$

where $0 \leq n \leq N-1$ is the domain of interest.

Let $y(n) = x(n-\tau)$ in equation 5.2. When τ=0, signal $x(n)$ and $x(n-\tau)$ are identical. The inner product (equation 5.2) is at a maximum. In general, the shift parameter between two signals always occurs at the peak of cross correlation. Compared to equation 5.2, the cross correlation (equation 5.1) is actually the inner product of $x(n)$ and $y(n)$, which is a function of shift parameter τ. Therefore, the cross correlation, like other inner products, measures the degree of similarity between two signals. In general, the cross correlation function is neither symmetrical, nor unimodal [Silvia, 1986]. Examples of this in ultrasonics show methods to select peaks [Sun, 2002].

The cross correlation is used to measure the relative time delay to a reference signal that results from the elastic wave propagation through a water path. An unknown signal, which is from the wave that propagates through the sample, is compared to this known signal. The relative time delay is determined by locating the time at which the cross-correlation r_{xy} is at a maximum. This is the point when the signals are most similar. The average group velocity V of the ultrasonic waves propagating through the sample can be estimated by [Hosten, 2001], as explained in section 3.3.1

$$V_i(x_1,\varphi) = \frac{V_0}{\sqrt{1+\frac{V_0\tau_i}{d}\left[\frac{V_0\tau_i}{d}-2\cos\theta_i\right]}} \qquad 5.3$$

where V_0 is the wave velocity in the water, τ_i is time delay, θ_i is the incident angle, d is the thickness of the sample, and (x_1, φ) indicates the wave incident plane.

It is important to note that the use of the cross correlation results only in a measure of the relative difference in the velocity. Therefore, the cross correlation can be used to determine the difference in wave velocity between the reference sample and the unknown sample. For the range of velocities considered, the only geometrical dispersion that would only impact the measurement exists if large differences in the phase velocities present between the unknown and the reference signal [Peterson, 1997]. As a result, unlike absolute measurements of velocity even in finite specimens, the effect of dispersion can be assumed to be minimal.

5.2 Attenuation Measurement

It is necessary to use deconvolution to remove the effects of the measurement system to allow determination of the attenuation of the ultrasonic wave propagating through the sample. Consider the configuration shown in Figure 5.1 [Schmerr, 1998]. In order to separate the effect of the sample on the ultrasonic wave, it is necessary to remove the response of the transducers and the rest of the measurement system from the test.

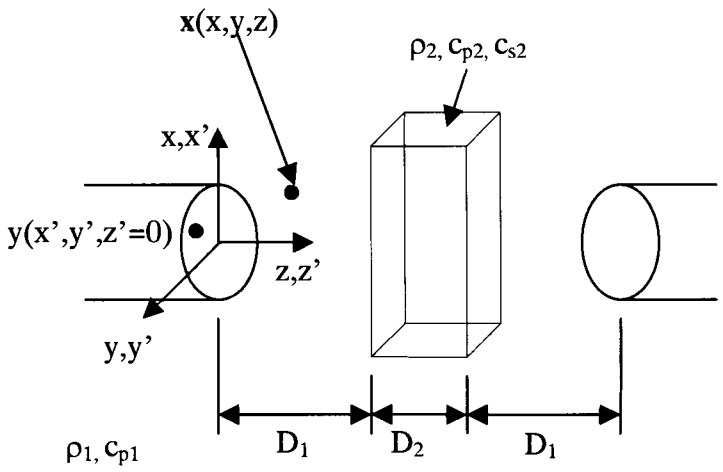

Figure 5.1 Immersion testing geometry [Schmerr, 1998]

In the configuration we consider the whole setup is immersed in water as a coupling fluid. In this setup an input voltage $V_i(t)$ drives the transducer, which converts electrical energy into mechanical motion. It is assumed that this transducer motion is a spatially uniform velocity $v_0(t)$ over the face of the transducer whose frequency components $v_0(\omega)$ are proportional to frequency components of the input voltage $V_i(\omega)$ [Schmerr, 1998], so that

$$\rho_1 c_{p1} v_0(\omega) = \beta_i(\omega) V_i(\omega) \qquad 5.4$$

where $\beta_i(\omega)$ is a frequency dependent input proportionality factor and ρ_1 and c_{p1} are the density and wave speed of the fluid surrounding the transducer respectively. During the reception process by the receiving transducer we assume that measured frequency components of the output voltage $V_0^m(\omega)$ are proportional to frequency components of the pressure received, $p_{ave}^m(\omega)$, defined as $V_i(\omega)$ [Schmerr, 1998]

$$p_{ave}^{m}(\omega) = \frac{1}{S_f} \int_{S_f} p(\vec{x},\omega)\, dS(\vec{x}) \tag{5.5}$$

where $p(\vec{x},\omega)$ is the pressure on the transducer face and S_f is the surface area of the transducer face. The above expression can also be written in terms of ideal received pressure $p_{ave}(\omega)$ as $V_i(\omega)$ [Schmerr, 1998]

$$p_{ave}^{m}(\omega) = p_{ave}(\omega)\exp\left[-\sum_{i=1}^{n}\alpha_i\, d_i\right] \tag{5.6}$$

where α_i and d_i are attenuation coefficients and corresponding path lengths followed by waves in the *i*th medium while travelling from the transmitter to the receiver. This decomposition is made so that $p_{ave}(\omega)$ is separated from the attenuation terms. The frequency components of the measured output voltage $V_0^m(\omega)$ can be written as $V_i(\omega)$ [Schmerr, 1998]

$$V_0^m(\omega) = \beta_r(\omega) p_{ave}(\omega)\exp\left[-\sum_{i=1}^{n}\alpha_i(\omega)\, d_i\right] \tag{5.7}$$

where $\beta_r(\omega)$ is a receiving proportionality factor. Combining equations 5.4 and 5.7 we get $V_i(\omega)$ [Schmerr, 1998]

$$V_0^m(\omega) = \beta(\omega)\left[\frac{p_{ave}(\omega)}{\rho_1 c_{p1} v_0(\omega)}\right]\exp\left[-\sum_{i=1}^{n}\alpha_i(\omega)\, d_i\right] \tag{5.8}$$

where $\beta(\omega)$ is single total efficiency factor

$$\beta(\omega) = \beta_i(\omega)\, \beta_r(\omega)\, V_i(\omega) \tag{5.9}$$

Using the general model, specific to the configuration in Figure 5.1 for measuring material attenuation [Schmerr, 1998] for both front and back surface responses we have

$$V_0^{fs}(\omega) = \beta(\omega)\left[\frac{P_{ave}^{fs}(\omega)}{\rho_1 c_{p1} v_0(\omega)}\right]\exp(-2\alpha_w D_1) \tag{5.10}$$

$$V_0^{bs}(\omega) = \beta(\omega)\left[\frac{P_{ave}^{bs}(\omega)}{\rho_1 c_{p1} v_0(\omega)}\right]\exp(-2\alpha_w D_1 - 2\alpha_s D_2) \tag{5.11}$$

V_0^{fs} and V_0^{bs} are measured output voltages of the front surface and back surface respectively. α_w and α_s are attenuation coefficients for the water and the solid. $\beta(\omega)$ is a receiving proportionality factor. The terms p_{ave}^{fs} and p_{ave}^{bs} are spatially averaged received pressure for the front-surface and back-surface, and v_0 is the frequency response of the spatially uniform velocity over the face of the transducer. The density and wave speed of the fluid surrounding the transducer are ρ_1 and c_{p1}. D_1 is the distance between the transducer and sample, and D_2 represents the thickness of the sample [Schmerr, 1998]. It is assumed that both front and back responses are measured with the same transducer and at the same system settings, so that the efficiency factor is the same in both cases. In principle we can obtain the attenuation of solid from Equation 5.10 by simply dividing the magnitudes of the back and front surface responses to obtain [Schmerr, 1998]

$$\exp(-2\alpha_s D_2) = \frac{|B(\omega)|}{|F(\omega)|} \tag{5.12}$$

where

$$|B(\omega)| = \left|V_0^{bs}(\omega) R_{12}^{p;p} D_p\left[\frac{k_{p1}a^2}{2D_1}\right]\right| \tag{5.13}$$

$$|F(\omega)| = \left|V_0^{fs}(\omega) T_{12}^{p;p} R_{21}^{p;p} T_{21}^{p;p} D_p\left[\frac{k_{p1}a^2}{2\overline{D}}\right]\right| \tag{5.14}$$

$R_{12}^{p:p}, T_{12}^{p:p}, and\ T_{21}^{p:p}$ denote the reflection coefficient from fluid to solid, the transmission coefficient from fluid to solid, and the transmission coefficient from solid to fluid, respectively. All of these three coefficients denote the transmitted longitudinal wave due to an incident longitudinal wave. D_l is a diffraction correction term, and $k_{p1} = \omega / c_{p1}$. An example of results of using such an approach for a block of aluminum is shown in Figure 5.2, where over a frequency range of 6-10 MHz, the attenuation variation can be fit to linear function as

$$\alpha(f) = 0.193f + 2.97 \quad \text{Np/m} \qquad 5.15$$

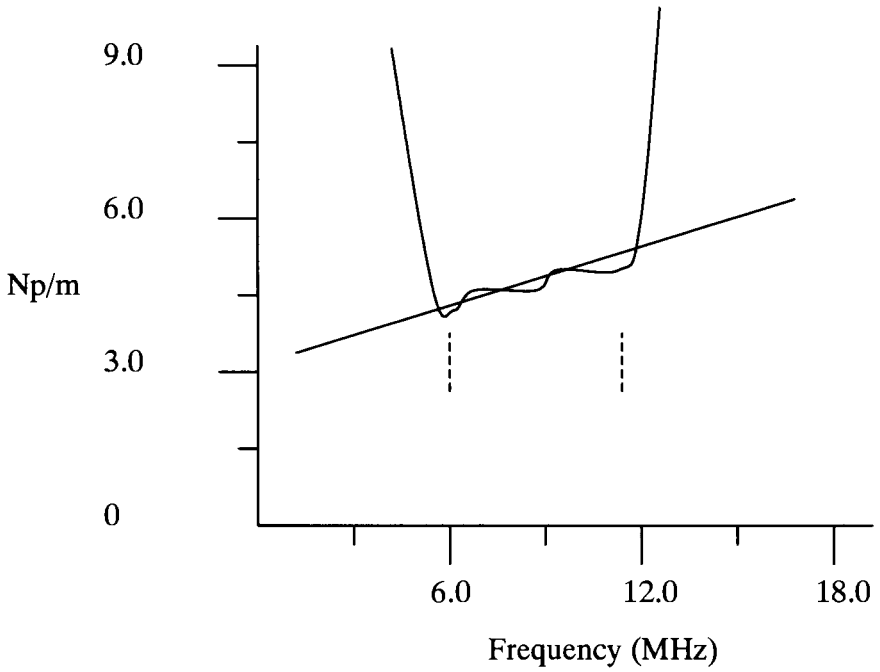

Figure 5.2 Attenuation coefficient as measured for an aluminum block and the best fit straight line for values in the bandwidth of the transducer (approximately 6-10 MHz) [Schmerr, 1998]

In this thesis equation 5.12 is used to calculate α_s from the measured signals $B(\omega)$ and $F(\omega)$. Plotting of the attenuation function is not done in this thesis.

5.3 Constrained Optimization

The next key element to the processing of the data is the optimization used to extract elastic constants from 100 experimental data sets. In general optimization arises whenever there is an objective function that must be tuned for optimal performance. Constrained optimization is the minimization of an objective function subject to constraints on the possible values of the independent variable. Constraints can be either equality constraints or inequality constraints. In this thesis, optimization is used to find the compliance tensor from velocity data measured in composite materials. The elastic constants are reconstructed from a large number of wave velocity data points, by performing Newton-Raphson non-linear optimization. The equation for optimization is

$$\left|\Gamma_{ij} - \delta_{ij}\rho V^2\right| = 0 \qquad 5.16$$

Three phase velocities corresponding to the three wave modes form the three solutions of this non-linear cubic equation (equation 3.18). Every measured phase velocity, V, is approximately the solution of equation 5.16.

$$f(V_{\exp}, C_{ij}) = \left|\Gamma_{ij} - \delta_{ij}\rho V^2\right| \cong 0 \qquad 5.17$$

where $f(V_{\exp}, C_{ij})$ is the left hand side of the equation 5.16 and $V_{\exp}(n)$ indicates the phase velocities measured from the four incident planes as described in section 4. Reconstruction of all 21 components of C_{ij} can be performed by minimizing an objective function $F(C_{ij})$, which is the sum of squares of equation 5.16.

$$C_{ij} = \min\left\{F(C_{ij})\right\} \qquad 5.18$$

with

$$F(C_{ij}) = \sum_{i=1}^{n} \left[f(V_{\exp}(i), C_{ij}) \right]^2 \qquad 5.19$$

where n represents all data points collected from the four incident planes.

Equation 5.19 shows that the method minimizes the effect of random deviations of experimental data on the results of reconstruction. The wave velocity measurements are indeed embodied in each objective function to be minimized. There are more experimental data points than the number of the independent elastic constants. Therefore Equation 5.17 is constructed from an over-determined system of the functions $f(V_{\exp}, C_{ij})$ [Every and Saches, 1990]. Contrary to another method that considers the direct solutions of Christoffel's equation [Rokhlin and Wang, 1992], this minimization problem requires no mode distinction [Aristegui and Baste, 1997]. This is simply because each of the modes generated is the solution of Christoffel's Equation and should satisfy Equation 5.16. For the general case, the velocity data are collected from four incident planes 0^0, 45^0, 90^0 and 135^0 associated with various incident angles.

The minimization was performed by using a standard MATLAB optimization function, which is based on the Newton-Raphson method described above. A successful implementation of optimization requires reasonable estimates of the elastic constants as initial values to feed into the algorithm. The determination of initial values was earlier explained in section 4.2.1.3.

The following steps leads to the reconstruction of the elastic constants C_{ij} using the optimization technique:

- A set of phase velocities $V_{exp}(1),...V_{exp}(n)$, which correspond to each of these wave modes, is measured from four incident planes. Twenty-five different incident angles are needed at each of the four incidental planes to make up a total of 100 data points.
- Using a trial set of elastic constants C^0_{ij} as an initial guess to construct a $f^0(V_{exp}, C^0_{ij})$, and an objective function $F^0(C_{ij})$ to be minimized through Equation 5.17 and Equation 5.19.
- At each step (kth) of the iteration, an error e_k, which is defined as the difference between the C_{ij}^k and the desired C_{ij}, will result. The closer the C_{ij}^k are to the C_{ij}, the smaller, on the average, the error will be.
- This procedure may be iterated until

$$e_k - e_{k-1} = C_{ij}^{(k)} - C_{ij}^{(k-1)} \leq \varepsilon \qquad 5.20$$

where ε is a pre-assigned tolerance of a very small quantity. An example is shown in the appendix.

6 RESULTS

This section provides summary results for the data obtained for the thesis and additional data may be found in the appendix. The coordinate system defined in section 3.3.1 is used in the discussion.

6.1 Results for Recovered Elastic Stiffness Tensor and Principal Coordinate System

6.1.1 Results for RCC

The initial guess used in the recovery of the elastic tensor from the ultrasonic data is obtained experimentally as illustrated in section 4.2.2.3 and is used in the recovery of the elastic stiffness tensor from the velocity data.

Initial guess, C =

$$\begin{bmatrix} 12.6199 & 4.4797 & 5.1299 & 0 & 0 & 0 \\ 4.4797 & 19.7806 & 7.2781 & 0 & 0 & 0 \\ 5.1299 & 7.2781 & 42.4375 & 0 & 0 & 0 \\ 0 & 0 & 0 & 4.0223 & 0 & 0 \\ 0 & 0 & 0 & 0 & 6.2121 & 0 \\ 0 & 0 & 0 & 0 & 0 & 13.7804 \end{bmatrix} \text{Gpa}$$

An example of the stiffness tensor reconstructed from the above initial guess using the velocity data is, stiffness tensor, C =

$$\begin{bmatrix} 19.7811 & 4.4791 & 7.2781 & 0.0005 & 0.0000 & -0.0535 \\ 4.4791 & 12.6206 & 5.1299 & 0.0009 & -0.0000 & 0.0847 \\ 7.2781 & 5.1299 & 42.4375 & 0.0043 & 0.0000 & 0.0094 \\ 0.0005 & 0.0009 & 0.0043 & 6.2121 & -0.0096 & -0.0000 \\ 0.0000 & -0.0000 & 0.0000 & -0.0096 & 4.0223 & -0.0017 \\ -0.0535 & 0.0847 & 0.0094 & -0.0000 & -0.0017 & 13.7798 \end{bmatrix} \text{Gpa}$$

The eigenvalues of C is

$$\text{eigenvalues(C)} = \begin{bmatrix} 45.7390 \\ 18.7190 \\ 10.3790 \\ 13.7830 \\ 6.2120 \\ 4.0220 \end{bmatrix} * 10^9$$

The reconstructed stiffness tensor has off diagonal terms which are represented as zeros but negative. These represent significantly small negative numbers in the tensor. The numbers are so small that they are assumed to be zero. As introduced in section 3.3.2, the principal coordinate system R^P with respect to the observation coordinate system R can be located by determining a set of Euler's angle unknowns $\delta=(\alpha, \beta, \gamma)$ with at least one of the unknown is zero [Auld, 1990; Aristegui and Baste, 1997]. For the stiffness tensor above, the Euler angles were determined to be

$$\alpha = 90^0$$
$$\beta = 91.79^0$$
$$\gamma = 0$$

Therefore, the principal system R^P was determined by a rotation through a counterclockwise angle $\alpha = 90^0$ about the $\vec{x}_3$ axis followed by another counterclockwise rotation through an angle $\beta = 91.79^0$ about the $\vec{x}_1$.

6.1.2 Results for e-glass Vinylester

The following is an example from the data obtained for the e-glass vinylester samples, with an initial guess [Peterson, et al., 2002], C =

$$\begin{bmatrix} 33.0027 & 13.7467 & 14.0248 & 0 & 0 & 0 \\ 13.7467 & 23.9168 & 11.2990 & 0 & 0 & 0 \\ 14.0248 & 11.2990 & 25.8612 & 0 & 0 & 0 \\ 0 & 0 & 0 & 4.7250 & 0 & 0 \\ 0 & 0 & 0 & 0 & 17.3210 & 0 \\ 0 & 0 & 0 & 0 & 0 & 14.5580 \end{bmatrix} \text{GPa}$$

An example of the stiffness tensor reconstructed using the initial guess, by performing a nonlinear optimization on the velocity data, is stiffness tensor, C =

$$\begin{bmatrix} 33.0646 & 13.9748 & 13.7087 & 0.0426 & -0.3409 & 0.5429 \\ 13.9748 & 25.9166 & 11.3053 & -0.0339 & 0.0013 & 0.3010 \\ 13.7087 & 11.3053 & 23.9629 & -0.0230 & 0.6592 & -0.0840 \\ 0.0426 & -0.0339 & -0.0230 & 4.7523 & -0.3412 & 0.4376 \\ -0.3409 & 0.0934 & 0.6592 & -0.3412 & 14.5110 & 0.0306 \\ 0.5429 & -0.7928 & -0.0840 & 0.4376 & 0.0306 & 17.2620 \end{bmatrix} \text{GPa}$$

For the stiffness tensor above the Euler angles were determined to be

$$\alpha = 182.48^0$$
$$\beta = 91.76^0$$
$$\gamma = 0$$

Data was collected form a sample, which was cut at an angle of 5 degrees from the x_2 direction. This was done in order to check the optimization routine. The reconstructed stiffness tensor, for this sample, C =

$$\begin{bmatrix} 33.1959 & 13.7853 & 13.7334 & -0.0102 & 0.2263 & -1.1910 \\ 13.7853 & 25.7867 & 11.5930 & -0.9112 & -0.0424 & 1.7409 \\ 13.7334 & 11.5930 & 23.7156 & 0.5028 & -0.3246 & 0.1901 \\ -0.0102 & -0.9112 & 0.5028 & 5.0649 & 0.7602 & -0.1507 \\ 0.2263 & -0.0424 & -0.3246 & 0.7602 & 14.5872 & -0.4750 \\ -1.1910 & 1.7409 & 0.1901 & -0.1507 & -0.4750 & 16.9962 \end{bmatrix} \text{ Gpa}$$

For the stiffness tensor above the Euler angles were determined to be

$$\alpha = 178.85^0$$
$$\beta = 8.56^0$$
$$\gamma = 0$$

Additional results are included in the appendix

6.2 Results for Damping Characteristics

Following selection of the principal axes of the sample it is now possible to measure damping using the one-dimensional theory presented in section 3. The damping characteristics of various samples and the repeatability of the process are considered. The following curves show the damping versus frequency characteristics for samples of RCC and e-glass vinylester. Repeatability of the experimental process is demonstrated in fig 6.2 and fig 6.4. Care was taken to make sure that the sample positioning on the sample holder was identical for all samples. Even though there are differences in the curves, all of them show the same trend. More data are plotted in the appendix section. A smoothed curve is also shown in the appendix section, which gives a better idea about the trend of these curves.

6.2.1 Results for RCC

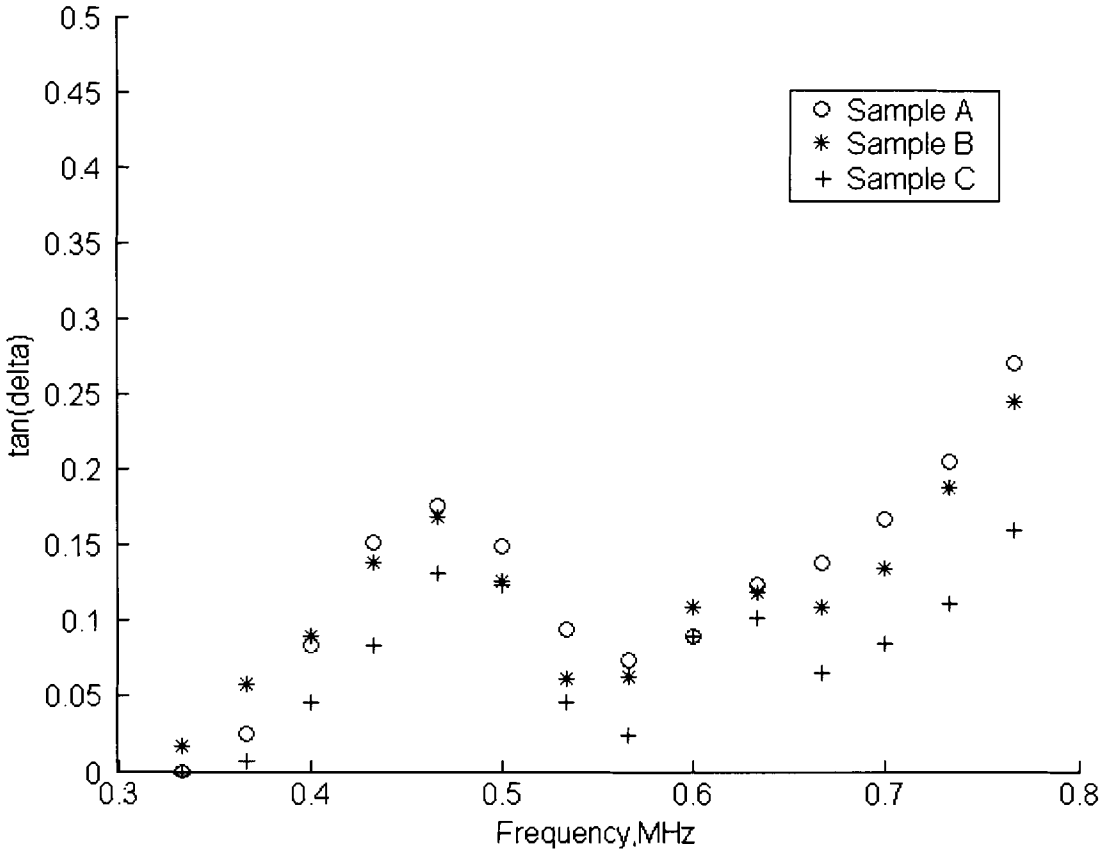

Figure 6.1 Damping characteristics of RCC, $\vec{x}_1$ direction for 3 specimens cut from the same sample

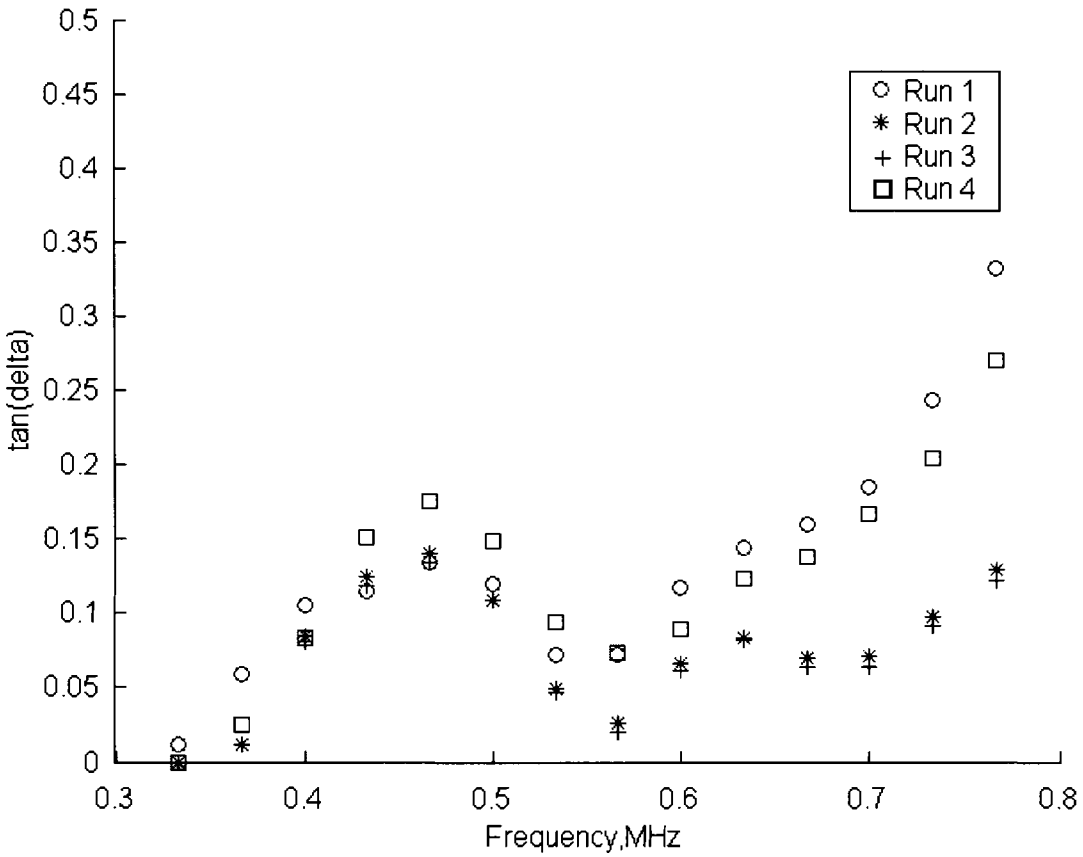

Figure 6.2 Repeatability of damping characterization of RCC, using the same sample in 4 different tests on different days under same conditions and same orientation

6.2.2 Results for e-glass Vinylester

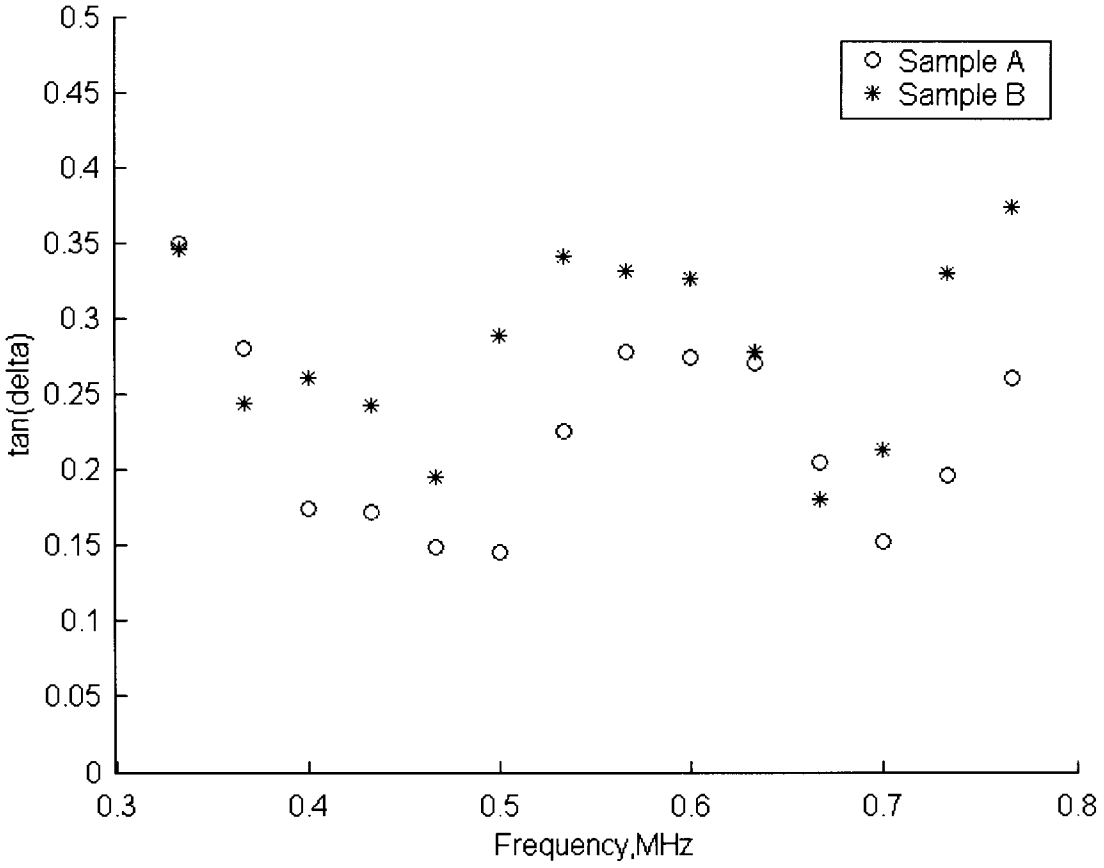

Figure 6.3 Damping characteristics of e-glass vinylester, $\bar{x}_1$ direction70

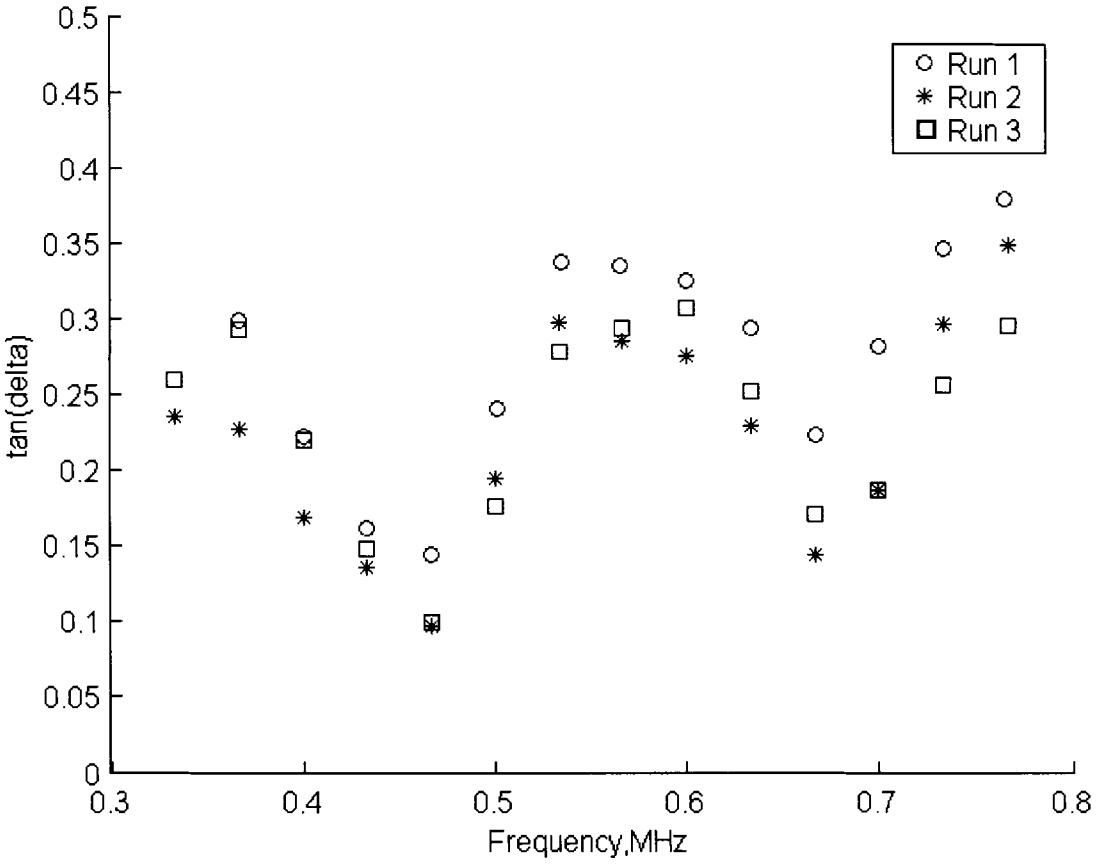

Figure 6.4 Repeatability of damping characterization process of e-glass vinylester, over 3 different runs on 3 different days under same conditions and same orientation

6.3 Effect of Oxidation on Damping

To study the effects of oxidation on damping of RCC samples, the difference in tan(δ) of the same sample before and after oxidation is studied at various frequencies. Five samples were considered with each oxidized to a different weight loss percentage. Figure 6.3 shows the variation in damping characteristics for samples oxidized to different levels.

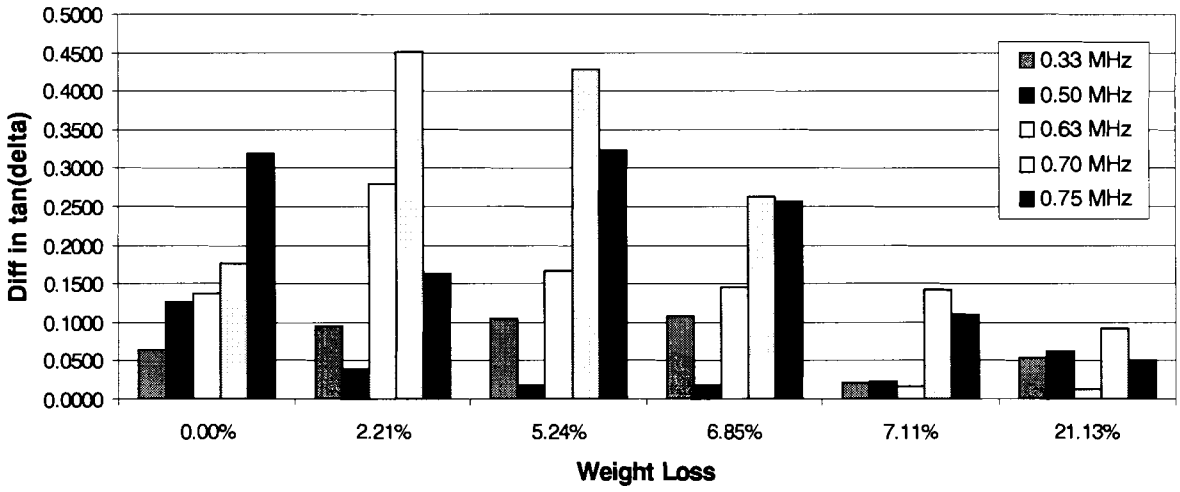

Figure 6.5 Attenuation changes during oxidation

7 DISCUSSIONS, CONCLUSION AND FUTURE WORK

From the results shown is section 6 it is clear that the measurement technique and the optimization routine used to recover the stiffness tensor from experimental data is working as expected. The recovered stiffness tensor is almost identical to the initial guess obtained using the contact method. This was expected since for both RCC and e-glass vinylester the samples were cut from a large composite sample. It was also demonstrated in the results that the composite samples are oriented with the principal axis and variability within 5°. This means for design it can be assumed orthotropic and simple measurements could be made with ultrasonic or other mechanical methods.

7.1 Stiffness Tensor recovered for RCC

For RCC the vector of eigenvalues is positive definite, which is a constraint on the optimization. Closer analysis of the initial guess and the recovered tensor for RCC in section 6.1.1 shows us that optimization routine found the minimum by flipping some of the terms. This is reasonable since it was possible that, while cutting the sample from the block for this particular experiment the orientations were switched with respect to the orientations of the sample used to find the initial guesses. When the optimization routine found the optimized value, it was in effect just changing the values in the $\vec{x}_1$ and $\vec{x}_2$ direction. The optimization routine ended up turning the axes by approximately 90° in the α and β directions, thereby orienting the samples in the same direction. For the composite samples we consider the initial guess to be in the principal axis

7.2 Stiffness Tensor recovered for e-glass Vinylester

The e-glass vinylester sample used in data collection was mis-oriented by 1.5° in the x_1 direction and 0.79° in the x_2 direction (section 6.1.2). Figure 7.1 illustrates this.

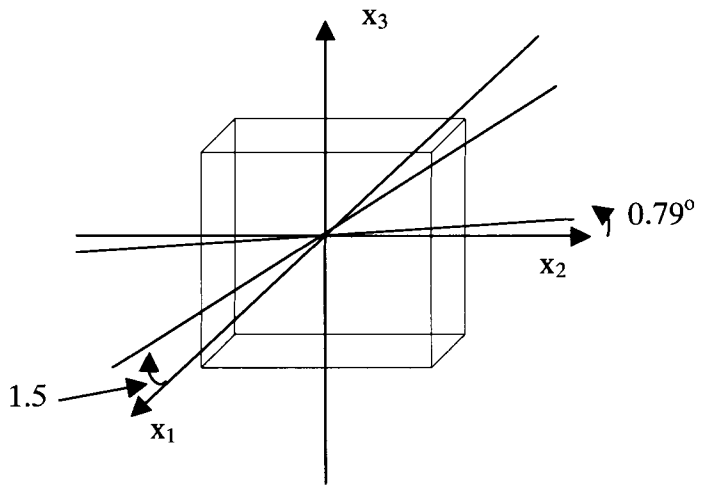

Figure 7.1 Orientation of the e-glass vinylester sample with respect to principal axis

Stiffness tensor recovered from the e-glass vinylester sample cut at an angle of 5 degrees off from the x_2 direction, was as expected. The Euler angle β was calculated to be 7.16°. This supports the optimization routine used to recover the stiffness tensor.

7.3 Damping Measurements and Oxidation Effects

The composite samples are oriented with the principal axis and varibility within 5°. The damping measurements were estimated with this variability. This was done because the variability is too small to cut the sample in the new orientation. Repeatability of the damping measurements is also acceptable with less than 10% variability. Improvements are needed to match design and evaluation state of matrix.

The attenuation changes during oxidation shown in Figure 6.5 shows similarity in trend with the initial results discussed in section 1.1.1. The difference in tan δ measurements for higher frequencies 0.75 MHz, 0.70 MHz and 0.63 MHz shows a decrease as oxidation is increased (increase in weight loss %). The two lower frequencies tend to have a wavy characteristic. This data is not suitable for designing until the damping accuracy is good.

7.4 Future Work

More work has to be done in the future to improve the techniques explained and developed in this thesis. The source of the variability in damping should be established. It can be due to boundary conditions, sample size, or the electronics used. Even though an efficient optimization routine is used, there are better techniques to tackle the problem [Venkataraman, 2002]. All these advanced optimization routines were not used in this thesis since they are beyond the scope of this research. Use of a better optimization package like TOMLAB® is also suggested.

REFERENCES

Achenbach, J. D. 1984. *Wave Propagation in ElasticSolids.* Amsterdam: Elsevier Science Publishers B.V.

Anastasi, R.F., Friedman, A., Hinders, M., and Madaras, E. 1998. NDE of damage in thick stitched composites using laser based ultrasound with optical fibers for remote generation and detection. *Material Evaluation*, Vol. 56. No 12.

Aristegui, C. and Baste S. 1997. Optimal determination of the material symmetry axes and associated elasticity tensor from ultrasonic velocity data. *Journal of the Acoustical Society of America.* Vol.102.

Aristegui C. and Baste, S. 2000. Determination of the elastic symmetry of a monolityic ceramic using bulk acoustic waves. *Journal of Nondestructive Evaluation.* Vol. 19.

Auld, B. A. 1990. *Acoustic Fields and Waves in Solids.* Malabar: Krieger Publishing Company.

Baudouin, S. and Hosten, B. 1997. Comparison between prediction and measurement of viscoelastic moduli in composite materials versus temperature using ultrasonic immersion technique with oil. *Journal of the Acoustical Society of America*, Vol. 102. No 6.

Bicerano, J. 1993. *Prediction of Polymer Properties.* New York: Marcel Dekker Inc.

Birman, V and Byrd, L. W. 2000. Review of *Fracture and fatigue in ceramic matrix composites, ASME Review papers in Applied Mechanics*, Vol. 53. No 6.

Bunker, S.P. 2002. Evaluation of Dynamic properties of Carbon-carbon Composite at Elevated Temperatures. Master's thesis, University of Maine.

Chimenti, D.E. 1997. Guided waves in plates and their use in materials characterization. *Applied Mechanics Reviews.* Vol. 50. No 5.

Christensen, R. M. 1971. *Theory of Viscoelasticity: An Introduction.* New York: Academic Press.

Chu, Y. C., Degtyar, A.H., and Rokhlin, S. I. 1994. A method for determination of elastic constants of a unidirectional lamina from ultrasonic bulk velocity measurements. *Journal of the Acoustical Society of America.* Vol. 96.

Cowin, S. C. and Mehrabadi, M. M. 1987. On the identification of material symmetry for anisotropic elastic materials. *Quarterly Journal of Mechanics and Applied Mathematics.* Vol. 40.

Cowin, S. C. 1989. Properties of the anisotropic elasticity tensor. *Quarterly Journal of Mechanics and Appied Mathematics.* Vol. 42.

Every, A. G. and Saches, W. 1990. Determination of the elastic constants of anisotropic solids from acoustic-wave group-velocity measurements. *Physics Review.* Vol. B42.

Fedorov, F. I. 1986. *Theory of Elastic Waves in Crystals.* New York: Plenum Press.

Fraga, A. N., Alvarez V. A., and Vazquez, A. 2003. Relationship between dynamic mechanical properties and water absorption of unsaturated polyester and vinyl ester glass fiber composites. *Journal of Composite Materials.* Vol. 30. No 17.

Fung, Y. C. 2001. *Classical and Computational Solid Mechanics*. Singapore: World Scientific.

Gauthier, M.M. 1995. *Carbon-Carbon Composites, Engineering Materials, Handbook Desk Edition*, Materials Park: ASM International.

Gehman, Jr., H. W., Barry, J. L., and Deal, D.W. 2003. Columbia Accident Investigation Board Report. *NASA*. Vol. 1.

Grigoriev, I. S. and Meilikhov, E. Z. 1997. *Handbook of Physical Quantities.* New York: CRC Press.

Hearmon, R. F. S. 1961. *An Introduction to Applied Anisotropic Elasticity*. London: Oxford University Press.

Hellier, C. J. 2001. *Handbook of Nondestructive Evaluation.* New York: McGraw-Hill.

Hellwege, K. H. 1979. *Numerical Data and Functional Relationships in Science and Technology Vol. 11*. New York: Springer-Verlag.

Hosten, B. 1991. Reflection and transmission of acoustic plane waves on an immersed orthotropic and viscoelastic solid layer. *Journal of the Acoustical Society of America.* Vol. 89.

Hosten, B. 2001. Ultrasonic Through-Transmission Method for measuring the complex stiffness moduli of composite materials. *Handbook of Elastic Properties Solids, Liquids, and Gases*. New York: Academic Press.

Hosten, B., Hutchins, D. A., and Schindel, D. W. 1996. Measurement of Elastic Constants in Composite Materials Using Air-Coupled Ultrasonic Bulk Waves, *Journal of the Acoustical Society of America*. Vol. 99. No 4.

Jenkins, C. H. 1998. *Manual on experimental methods of mechanical testing of composites.* Lilburn: The Fairmont Press, Inc.

Jones, R. M. 1975. *Mechanics of composite materials.* New York: Hemisphere Publishing Corporation.

Kimura, S., Yasuda, E., and Tanabe, Y. 1982. *Microstructure and Fracture Behavior of Unidirectionally Reinforced Carbon Fiber/Carbon Composites.* Progress in Science and Engineering of Composites International Conference.

Krautkramer, J. and Krautkramer, H. 1975. *Ultrasonic testing of materials (Third, revised edition).* New York: Springer-Verlag.

Mase, G. E. 1970. *Schaum's Outline of: Theory and Problems of Continuum Mechanics.* New York: McGraw-Hill Book Co.

Menard, K. P. 1999. *Dynamic Mechanical Analysis: A Practical Introduction.* Boca Raton: CRC Press.

Migliori, A. and Sarrao, J. L. 1997. *Resonant ultrasound spectroscopy.* New York: Wiley.

Musgrave, M. J. P. 1970. *Crystal Acoustics.* San Francisco: Holden-Day, Inc.

Newman, J. W., 1996. Shearography. Non destructive testing for aerospace composites. *Trends in NDE science & technology; Proceedings of the 14th World conference on non destructive testing.* New Delhi.

Norris, A. N. 1988. On the acoustic determination of the elastic moduli of anisotropic solids and acoustic conditions for the existence of planes of symmetry. *Quarterly Journal of Mechanics and Applied Mathematics.* Vol. 42.

Papadakis, E. P., Patton, T., Tsai, Y. M., Thompson, D. O., and Thompson, R. B. 1991. The elastic moduli of a thick composite as measured by ultrasonic bulk wave pulse velocity. *The Journal of the Acoustical Society of America.* Vol. 89.

Peterson, M. L. 1997. A Method for Increased Accuracy of the Measurement of Phase Velocity. *Ultrasonics.* Vol. 35. No 1.

Peterson, M. L., Sun, M., Senan, A., Horton, K., Radford, D. W., and Thompson, L., 2002. Dynamic Materials Characterization of Marine Composites. *17th Technical Conference, American Society for Composites.* Lafayette.

Rokhlin, S. I. and Wang, W. 1992. Double Through-Transmission Bulk Wave Method for Ultrasonic Phase Velocity Measurement and Determination of Elastic Constants of Composite Materials. *Journal of the Acoustical Society of America.* Vol. 91. No 6.

Savage, G. 1993. *Carbon-Carbon Composites.* London: Chapman & Hall.

Schmerr, Jr., L. W. 1998. *Fundamental of Ultrasonic Nondestructive Evaluation; A Modeling Approach.* New York: Plenum Press.

Schreiber, E., Aderson, O., and Soga, N. 1973. *Elastic Constants and Their Measurements.* New York: McGraw-Hill.

Shames, I. H. 1966. *Engineering Mechanics Vol. II Dynamics.* New Jersey: Prentice-Hall, Inc.

Silvia, M. T. 1986. *Handbook of Digital Signal Processing: Time Delay Estimation* Chapter 11. New York: Academic Press, Inc.

Strobl, G. 1996. *The Physics of Polymers: Concepts for understanding their Structures and Behavior*. New York: Springer.

Summerscales, J. 1990. *Non-destructive testing of fiber-reinforced plastic composites Vol. 2.* New York: Elsevier Science Publishing Co., Inc.

Sun, M. 2002. Optimal recovery of elastic properties for a general anisotropic material through ultrasonic measurements. Master's thesis, University of Maine.

Venkataraman, P. 2002. *Applied Optimization with MATLAB Programming.* New York: John Wiley & Sons.

Zweschper, T., Dillenz, A., Riegert, G., Scherling, D., and Busse, G. 2003. Ultrasound excited thermography using frequency modulated elastic waves, *Insight - Non-Destructive Testing and Condition Monitoring,* Vol. 45. No 3.

APPENDICES

Appendix A – MatLab Routines

Optimization Routine Used to Recover the Stiffness tensor

Following are the MATLAB routines and functions used to obtain the elastic tensor from the velocity data.

```
clear;
format('short');
%initial guess
guess_ec=[121.3977  45.8033  50.1603  0        0        0;
           45.8033  69.8789  34.7046  0        0        0;
           50.1603  34.7046  105.0708 0        0        0;
            0        0        0       27.6067  0        0;
            0        0        0       0        16.5485  0;
            0        0        0       0        0        26.5371]*10^9;

c=guess_ec;

%Input Options
%Tolerances and Iteration limits can be set using this
%options=optimset('MaxFunEvals',18000,'MaxIter',1000,'MaxPCGIter',1000,'LargeScale','on','TolX',1e+7
,'TolCon',1e+7);
%%%%%%%%%%%%%%%%%%%%%%%%%%%%%%%% Optimization
%%%%%%%%%%%%%%%%%%%%%%%%%%%%%%%%%%%%
% (@Get_object_F_eg_b -- Our function which takes in an initial value for EC &
% computes through and gives out the velocities obtained to give a better EC
%guess_ec -- Initial value of EC
%0 -- Minimum value possible for any entry in the EC matrix
%14*10^9 -- Maximum value possible for any entry in the EC matrix
%options -- Sets the tolerences and maximum iteration values for optimization
%%%%%%%%%%%%%%%%%%%%%%%%%%%%%%%%%%%%%%%%%%%%%%%%%%%%%%%%%%%%%%%%%%%%%%%%%%%%%%%
%%%%%%%%%%%%%%%%%%%%%%%%%%%%%%%%%%%%
%EC_arbiary=lsqnonlin(@Get_object_F_eg_b,guess_ec,-0.00001,129*10^9,options);

EC_arbiary(2,1)=EC_arbiary(1,2);
EC_arbiary(3,1)=EC_arbiary(1,3);
EC_arbiary(3,2)=EC_arbiary(2,3);
EC_arbiary(4,1)=EC_arbiary(1,4);
EC_arbiary(4,2)=EC_arbiary(2,4);
EC_arbiary(4,3)=EC_arbiary(3,4);
EC_arbiary(5,1)=EC_arbiary(1,5);
EC_arbiary(5,2)=EC_arbiary(2,5);
EC_arbiary(5,3)=EC_arbiary(3,5);
EC_arbiary(5,4)=EC_arbiary(4,5);
EC_arbiary(6,1)=EC_arbiary(1,6);
EC_arbiary(6,2)=EC_arbiary(2,6);
EC_arbiary(6,3)=EC_arbiary(3,6);
```

```
EC_arbiary(6,4)=EC_arbiary(4,6);
EC_arbiary(6,5)=EC_arbiary(5,6);

c=EC_arbiary;

A=[c(1,1)+c(1,2)+c(1,3) c(1,6)+c(2,6)+c(3,6) c(1,5)+c(2,5)+c(3,5);
    c(1,6)+c(2,6)+c(3,6) c(1,2)+c(2,2)+c(2,3) c(1,4)+c(2,4)+c(3,4);
    c(1,5)+c(2,5)+c(3,5) c(1,4)+c(2,4)+c(3,4) c(1,3)+c(2,3)+c(3,3)];

B=[c(1,1)+c(5,5)+c(6,6) c(1,6)+c(2,6)+c(4,5) c(1,5)+c(4,6)+c(3,5);
    c(1,6)+c(2,6)+c(4,5) c(2,2)+c(4,4)+c(6,6) c(2,4)+c(3,4)+c(5,6);
    c(1,5)+c(4,6)+c(3,5) c(2,4)+c(3,4)+c(5,6) c(3,3)+c(4,4)+c(5,5)];

[vec_A,D_A]=eig(A);
[vec_B,D_B]=eig(B);
for i=1:3
 AdotB=dot(vec_A(:,i), vec_B(:,i));
 ampA=(sum((vec_A(:,1)).^2))^.5;
 ampB=(sum((vec_B(:,1)).^2))^.5;
 Agl(i)=acos((AdotB)/(ampA*ampB))*180/pi;
end

a=((vec_A+vec_B)/2);

for i=1:3
   alfa(i)=acos(a(1,i));
   if sin(alfa(i))==0
      beta(i)=0.0001;
   else
   beta(i)=acos((-a(2,i))/sin(alfa(i)));
   check(i)=sin(alfa(i))*sin(beta(i));
   alfa(i)=alfa(i)*180/pi;
   beta(i)=beta(i)*180/pi;
end
end

fprintf('\n\nalpha = %0.4f degrees\nbeta  = %0.4f degrees',alpha,beta);

Euler_alfa=alfa(3)
Euler_beta=beta(2)

%%%%%%%%%%%%%%%%%%%%%%%%%%
%%%%%%%%%%%%%%%%%%%%%%%%%%
%find EC in principal coordinate system
Agl_x=Euler_beta*pi/180;
Rota_X=[1        0          0;
     0        cos(Agl_x)     sin(Agl_x);
     0        -sin(Agl_x)    cos(Agl_x)];

a=Rota_X;
a_Sq=a.^2;

M_x=[ a_Sq(1,1:3)      2*a(1,2)*a(1,3)     2*a(1,3)*a(1,1)    2*a(1,1)*a(1,2);
       a_Sq(2,1:3)     2*a(2,2)*a(2,3)     2*a(2,3)*a(2,1)    2*a(2,1)*a(2,2);
       a_Sq(3,1:3)     2*a(3,2)*a(3,3)     2*a(3,3)*a(3,1)    2*a(3,1)*a(3,2);
       a(2,1)*a(3,1) a(2,2)*a(3,2) a(2,3)*a(3,3)    a(2,2)*a(3,3)+a(2,3)*a(3,2)
```

```
        a(2,1)*a(3,3)+a(2,3)*a(3,1)                    a(2,2)*a(3,1)+a(2,1)*a(3,2);
        a(3,1)*a(1,1) a(3,2)*a(1,2) a(3,3)*a(1,3)  a(1,2)*a(3,3)+a(1,3)*a(3,2)
        a(1,3)*a(3,1)+a(1,1)*a(3,3)     a(1,1)*a(3,2)+a(1,2)*a(3,1);
        a(2,2)*a(2,1) a(1,2)*a(2,2) a(1,3)*a(2,3)  a(1,2)*a(2,3)+a(1,3)*a(2,2)
        a(1,3)*a(2,1)+a(1,1)*a(2,3)     a(1,1)*a(2,2)+a(1,2)*a(2,1)];

%%%%%%%%%%%%%%%%%%%%%%%%%%%%%%%%%%%%%
Agl_z=Euler_alfa*pi/180;

Rota_Z=[cos(Agl_z)   sin(Agl_z)   0;
     -sin(Agl_z)  cos(Agl_z)   0;
     0        0         1]; %rotate about the z anix with clockwise 30
a=Rota_Z;
a_Sq=a.^2;

M_Z=[ a_Sq(1,1:3)      2*a(1,2)*a(1,3)     2*a(1,3)*a(1,1)    2*a(1,1)*a(1,2);
        a_Sq(2,1:3)      2*a(2,2)*a(2,3)     2*a(2,3)*a(2,1)    2*a(2,1)*a(2,2);
        a_Sq(3,1:3)      2*a(3,2)*a(3,3)     2*a(3,3)*a(3,1)    2*a(3,1)*a(3,2);
        a(2,1)*a(3,1) a(2,2)*a(3,2) a(2,3)*a(3,3)  a(2,2)*a(3,3)+a(2,3)*a(3,2)
        a(2,1)*a(3,3)+a(2,3)*a(3,1)    a(2,2)*a(3,1)+a(2,1)*a(3,2);
        a(3,1)*a(1,1) a(3,2)*a(1,2) a(3,3)*a(1,3)  a(1,2)*a(3,3)+a(1,3)*a(3,2)
        a(1,3)*a(3,1)+a(1,1)*a(3,3)    a(1,1)*a(3,2)+a(1,2)*a(3,1);
        a(2,2)*a(2,1) a(1,2)*a(2,2) a(1,3)*a(2,3)  a(1,2)*a(2,3)+a(1,3)*a(2,2)
        a(1,3)*a(2,1)+a(1,1)*a(2,3)    a(1,1)*a(2,2)+a(1,2)*a(2,1)];

v1=c/(M_x');
c_z1=inv(M_x)*v1;

v2=c_z1/(M_Z');
EC_prinpl=inv(M_Z)*v2;

c=EC_prinpl;
```

Function Used in the Optimization Routine

```
function F=Get_object_F_eg_b(guess_ec)
%This is a function intents to generate an object function for determination the elastic constants.
%F is based on the Christoffel's Equation

load d:\Usr\Anish\Research\Data\check\eglass\run1\sampleb\egb_velocityX0.dat;
load d:\Usr\Anish\Research\Data\check\eglass\run1\sampleb\egb_velocityX45.dat;
load d:\Usr\Anish\Research\Data\check\eglass\run1\sampleb\egb_velocityX90.dat;
load d:\Usr\Anish\Research\Data\check\eglass\run1\sampleb\egb_velocityX135.dat;

m=length(egb_velocityX0);
Agl=[0:m]';
Alfa=[Agl; Agl; Agl; Agl]*pi/180;
Density=2019.471308; %Kg/m^3

Velocity=[egb_velocityX0;egb_velocityX45;egb_velocityX90;egb_velocityX135];
RL_V_Sqr=(Density*(Velocity.^2));

Beta=[0;45;90;135]*pi/180;

for i=1:4*m
```

```
  index_Beta=1+floor((i-1)/25);
  n1(i)=sin(Alfa(i))*cos(Beta(index_Beta));
  n2(i)=sin(Alfa(i))*sin(Beta(index_Beta));
  n3(i)=cos(Alfa(i));
end

c=guess_ec;
for i=1:100
   T(1,1)=(n1(i)^ 2*c(1,1)+n2(i)^2*c(6,6) +n3(i)^2*c(5,5)+2*n2(i)*n3(i)*c(5,6)+ 2*n3(i)*n1(i)*
         c(1,5)+2*n1(i)*n2(i)*c(1,6))-RL_V_Sqr(i);
   T(1,2)=n1(i)^2*c(1,6)+n2(i)^2*c(2,6)+ n3(i)^2*c(4,5)+n2(i)*n3(i)*(c(4,6)+c(2,5))+ n3(i)*n1(i)*
         (c(1,4)+c(5,6))+n1(i)*n2(i)*(c(1,2)+c(6,6));
   T(2,1)=T(1,2);
   T(1,3)=n1(i)^2*c(1,5)+n2(i)^2*c(4,6)+ n3(i)^2*c(3,5)+n2(i)*n3(i)*(c(4,5)+ c(3,6))+n3(i)*n1(i)*
         (c(1,3)+c(5,5))+n1(i)*n2(i)*(c(1,4)+c(5,6));
   T(3,1)=T(1,3);
   T(2,2)=n1(i)^2*c(6,6)+n2(i)^2*c(2,2)+ n3(i)^2*c(4,4)+2*n2(i)*n3(i)*c(2,4)+ 2*n3(i)*n1(i)*
         c(4,6)+2*n1(i)*n2(i)*c(2,6)-RL_V_Sqr(i);
   T(2,3)=n1(i)^2*c(5,6)+n2(i)^2*c(2,4)+ n3(i)^2*c(3,4)+n2(i)*n3(i)*(c(4,4)+ c(2,3))+n3(i)*n1(i)*
         (c(3,6)+c(4,5))+n1(i)*n2(i)*(c(2,5)+c(4,6));
   T(3,2)=T(2,3);
   T(3,3)=n1(i)^2*c(5,5)+n2(i)^2*c(4,4)+ n3(i)^2*c(3,3)+2*n2(i)*n3(i)*c(3,4)+ 2*n3(i)*n1(i)*
         c(3,5)+2*n1(i)*n2(i)*c(4,5)-RL_V_Sqr(i);
   F(i)=det(T);
end
```

Routine Used to Determine the Velocities from Experimental Data

```
clear;
%Reference signal
load d:\USR\Anish\Research\Data\check\eglass\run5_10\x0\water_ref.out;
ref=water_ref(:,2);
n=length(ref);
V_ref=1485.7; %pick up the lowest sound speed in water, unit:m/s
Thickness=0.008788; %thickness of the sample, unit:m
timearray=water_ref(:,1);
interval=timearray(2)-timearray(1);

%Input first data file
load d:\USR\Anish\Research\Data\check\eglass\run5_10\x0\A100.out;
input(:,1)=A100(:,2);

%Input rest of the data files
fileNumber=24;
for i=1:fileNumber
   fileName=sprintf('%s%02d.out','d:\USR\Anish\Research\Data\check\eglass\run5_10\x0\A1',i);
   fileContent=load(fileName);
   input(:,i+1)=fileContent(:,2);
end

Agl=[0:24]*pi/180;

%Cross-correlation
for p=1:25
   for m=2:n
   shift_y1=[input((m:n),p);zeros(m-1,1)];
```

```
  cro1(p,m)=dot(ref,shift_y1);
  shift_y2=[ref(m:n);zeros(m-1,1)];
  cro2(p,m)=dot(input(:,p),shift_y2);
  end
  cro1(p,1)=dot(ref, input(:,p));
  cro2(p,1)=dot(input(:,p), ref);

  [y1,i1]=max(cro1(p,:));
  [y2,i2]=max(cro2(p,:));

  if y1>y2
    y(p)=y1;
    index_y(p)=-i1;
    cro(p,:)=cro1(p,:);
  else
    y(p)=y2;
    index_y(p)=i2;
    cro(p,:)=cro2(p,:);
  end

     delay(p)=interval*(index_y(p)-1);

  %%%Calculate velocities
   velocity(p)=V_ref/(1+V_ref*delay(p)/Thickness*(V_ref*delay(p)/Thickness-2*cos(Agl(p))))^.5;
   velocity1(p)=[(delay(p)/Thickness)^2-2*delay(p)*cos(Agl(p))/(V_ref*Thickness)+(1/V_ref)^2]^(-.5);
end
velocity;
%index_y
fid=fopen('d:\USR\Anish\Research\Data\check\eglass\run5_10\ega_velocityX0.dat','w');
fprintf(fid,'%16.12f\n',velocity);
fclose(fid);
```

Sample Data File

Time (s)	Voltage
0.00E+00	2.89E-04
2.00E-09	2.89E-04
4.00E-09	2.81E-04
6.00E-09	2.89E-04
8.00E-09	-1.56E-05
1.00E-08	1.33E-04
1.20E-08	2.81E-04
1.40E-08	1.33E-04
1.60E-08	1.33E-04
1.80E-08	-2.34E-05
2.00E-08	-1.56E-05
2.20E-08	2.81E-04
2.40E-08	1.25E-04
2.60E-08	1.33E-04
2.80E-08	2.81E-04
3.00E-08	-2.34E-05
3.20E-08	5.86E-04

Table A.1 Sample data file recorded using the oscilloscope

Appendix B - More Results and Smoothened Damping Curves

This section gives an account of various results obtained throughout the research period for stiffness tensor

Experiment date: 25/06/03

Sample: RCC 1A

$$C = \begin{bmatrix} 21.1500 & 2.6764 & 7.1479 & 0.0008 & 0.0004 & -0.4670 \\ 2.6764 & 14.8570 & 5.2601 & 0.0004 & -0.0009 & 0.1754 \\ 7.1479 & 5.2601 & 42.4375 & 0.0044 & 0.0001 & 0.5125 \\ 0.0008 & 0.0004 & 0.0044 & 6.0794 & -0.5224 & -0.0006 \\ 0.0004 & -0.0009 & 0.0001 & -0.5224 & 4.1550 & -0.0014 \\ -0.4670 & 0.1754 & 0.5125 & -0.0006 & -0.0014 & 11.9771 \end{bmatrix} \text{GPa}$$

Euler angles, $\alpha = 169.51^0$
$\beta = 89.36^0$
$\gamma = 0$

Experiment date: 07/07/03

Sample: RCC 2B

$$C = \begin{bmatrix} 19.7923 & 4.4724 & 7.2693 & 0.1475 & 0.0140 & -0.2667 \\ 4.4724 & 12.6656 & 5.1858 & 0.2606 & -0.0272 & 0.4213 \\ 7.2693 & 5.1858 & 42.3004 & 1.3020 & 0.0025 & 0.0481 \\ 0.1475 & 0.2606 & 1.3020 & 6.2660 & -0.0464 & -0.0222 \\ 0.0140 & -0.0272 & 0.0025 & -0.0464 & 4.0502 & -0.5108 \\ -0.2667 & 0.4213 & 0.0481 & -0.0222 & -0.5108 & 13.7385 \end{bmatrix} \text{GPa}$$

Euler angles, $\alpha = 91.47^0$
$\beta = 89.75^0$
$\gamma = 0$

Experiment date: 20/08/03

Sample: RCC 3B

$$C = \begin{bmatrix} 19.8217 & 4.4273 & 7.2737 & 0.0472 & -0.0083 & 0.5000 \\ 4.4273 & 12.6878 & 5.1390 & 0.0807 & 0.0161 & -0.7931 \\ 7.2737 & 5.1390 & 42.4238 & 0.4125 & -0.0015 & -0.0882 \\ 0.0472 & 0.0807 & 0.4125 & 6.2139 & 0.0895 & 0.0132 \\ -0.0083 & 0.0161 & -0.0015 & 0.0895 & 4.0286 & -0.1608 \\ 0.5000 & -0.7931 & -0.0882 & 0.0132 & -0.1608 & 13.7246 \end{bmatrix} \text{GPa}$$

Euler angles, $\alpha = 88.62^0$
$\beta = 89.75^0$
$\gamma = 0$

Experiment date: 10/03/03

Sample: e-glass vinylester 1A

$$C = \begin{bmatrix} 33.3733 & 13.7173 & 13.5685 & -0.0025 & -1.6560 & -0.0275 \\ 13.7173 & 23.9152 & 11.3307 & -0.0481 & 0.2665 & 0.0399 \\ 13.5685 & 11.3307 & 26.4003 & 0.0893 & 2.4336 & 0.0048 \\ -0.0025 & -0.0481 & 0.0893 & 4.8453 & 0.0182 & 1.0707 \\ -1.6560 & 0.2665 & 2.4336 & 0.0182 & 16.8670 & 0.0402 \\ -0.0275 & 0.0399 & 0.0048 & 1.0707 & 0.0402 & 14.4406 \end{bmatrix} \text{GPa}$$

Euler angles, $\alpha = 186.29^0$
$\beta = 90.75^0$
$\gamma = 0$

Experiment date: 10/08/03

Sample: e-glass vinylester 2B

$$C = \begin{bmatrix} 33.0710 & 13.7415 & 13.9407 & 0.0046 & -0.7278 & -0.0169 \\ 13.7415 & 23.9134 & 11.3088 & -0.0723 & 0.1143 & 0.0240 \\ 13.9407 & 11.3088 & 25.9552 & 0.1197 & 1.0612 & 0.0033 \\ 0.0046 & -0.0723 & 0.1197 & 4.7510 & 0.0113 & 0.4592 \\ -0.7278 & 0.1143 & 1.0612 & 0.0113 & 17.2386 & 0.0627 \\ -0.0169 & 0.0240 & 0.0033 & 0.4592 & 0.0627 & 14.5380 \end{bmatrix} \text{ GPa}$$

Euler angles, $\alpha = 182.68^0$

$\beta = 91.33^0$

$\gamma = 0$

This section shows the smoothened curves of damping accuracy and damping repeatability using a second-degree polynomial curve fit.

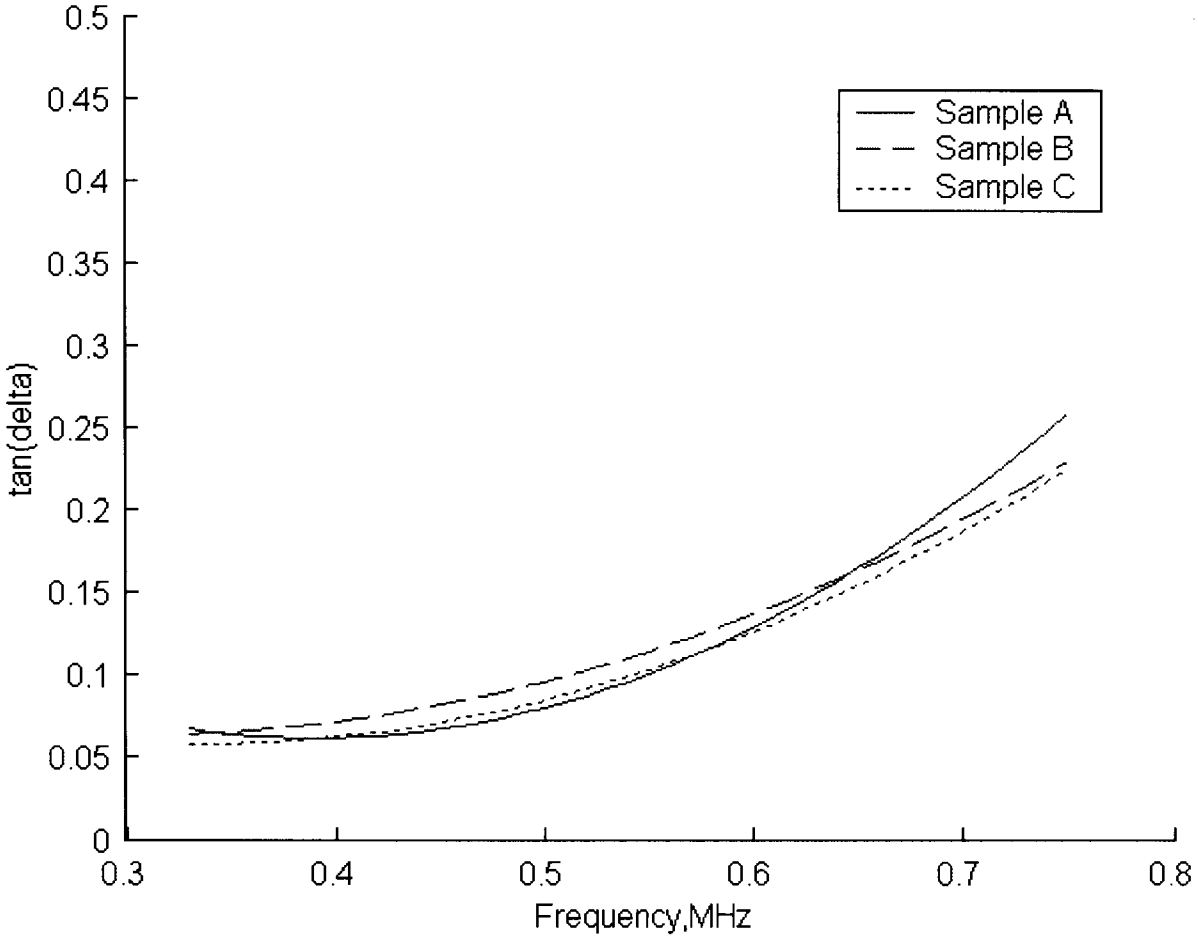

Figure B.1 Damping characteristics of RCC, x_1 direction, smoothened curve

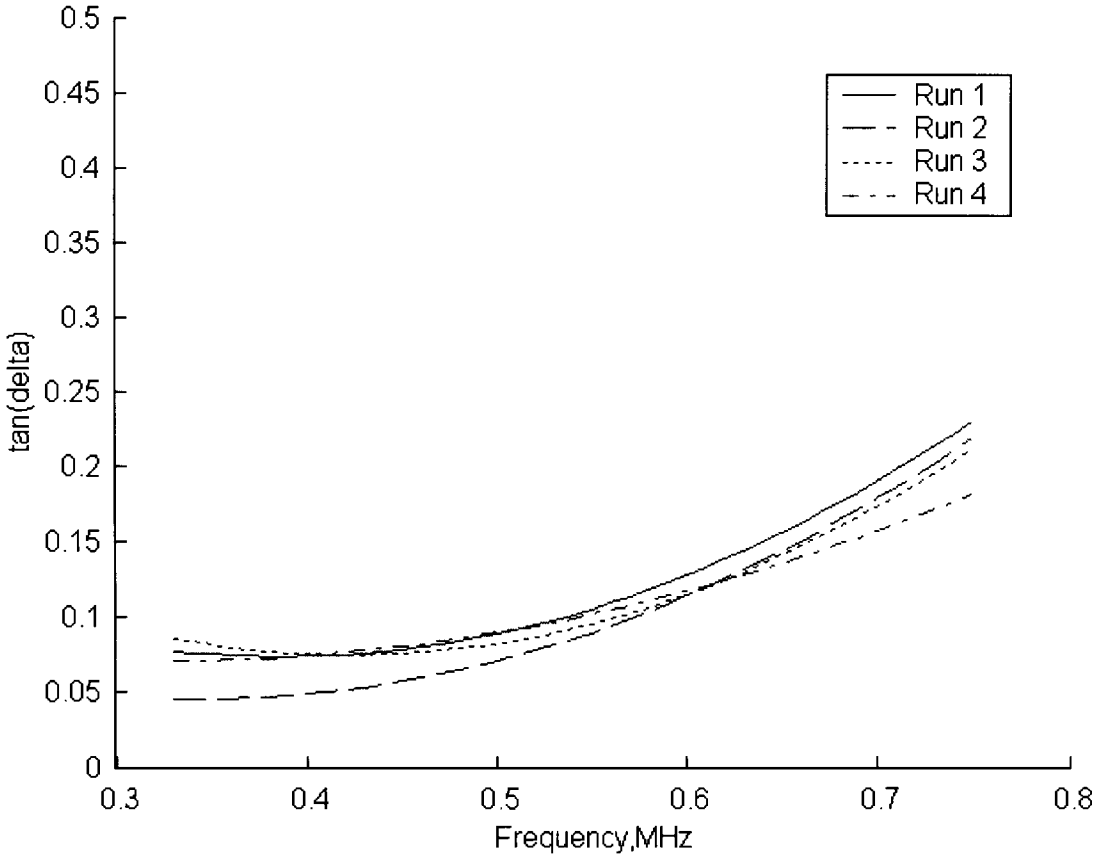

Figure B.2 Smoothened curve showing repeatability of damping characterization process, over 4 different runs on 4 different days under same conditions and same orientation for RCC

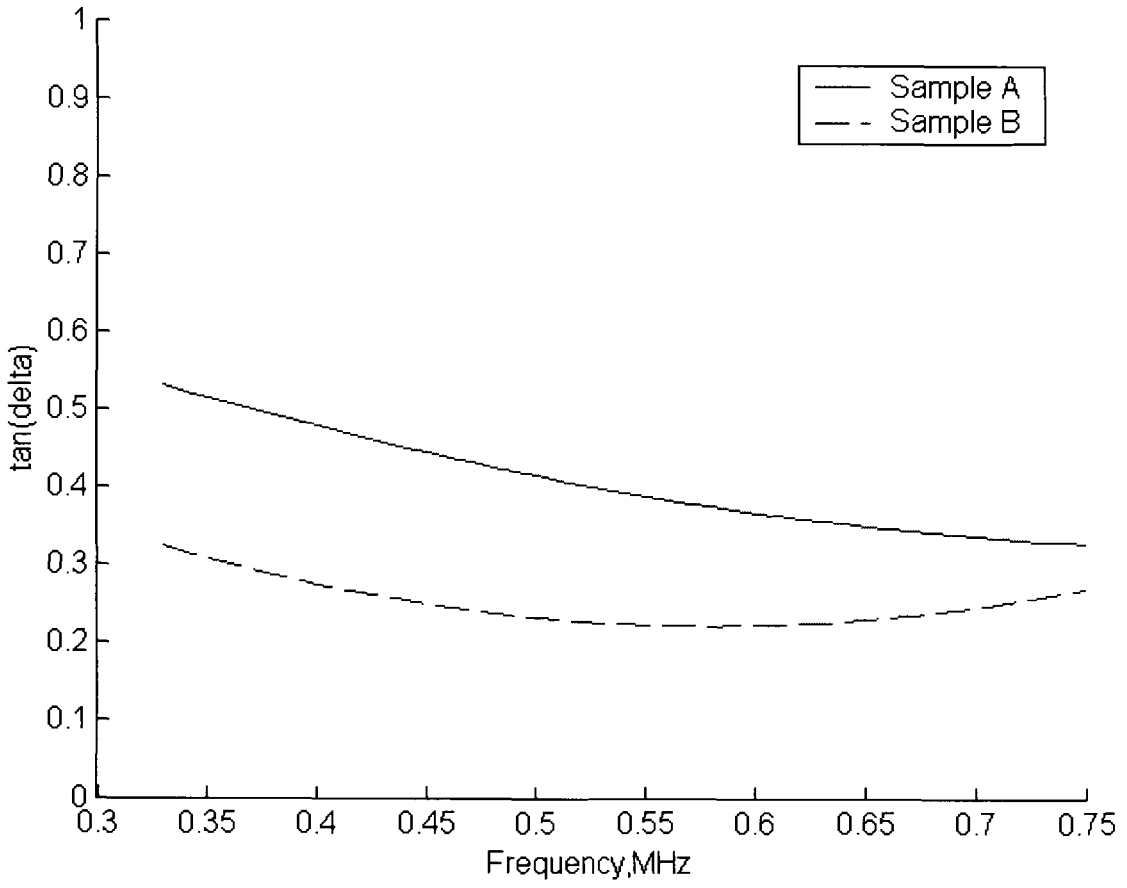

Figure B.3 Smoothened curve of damping characteristics of e-glass vinylester in x_1 direction

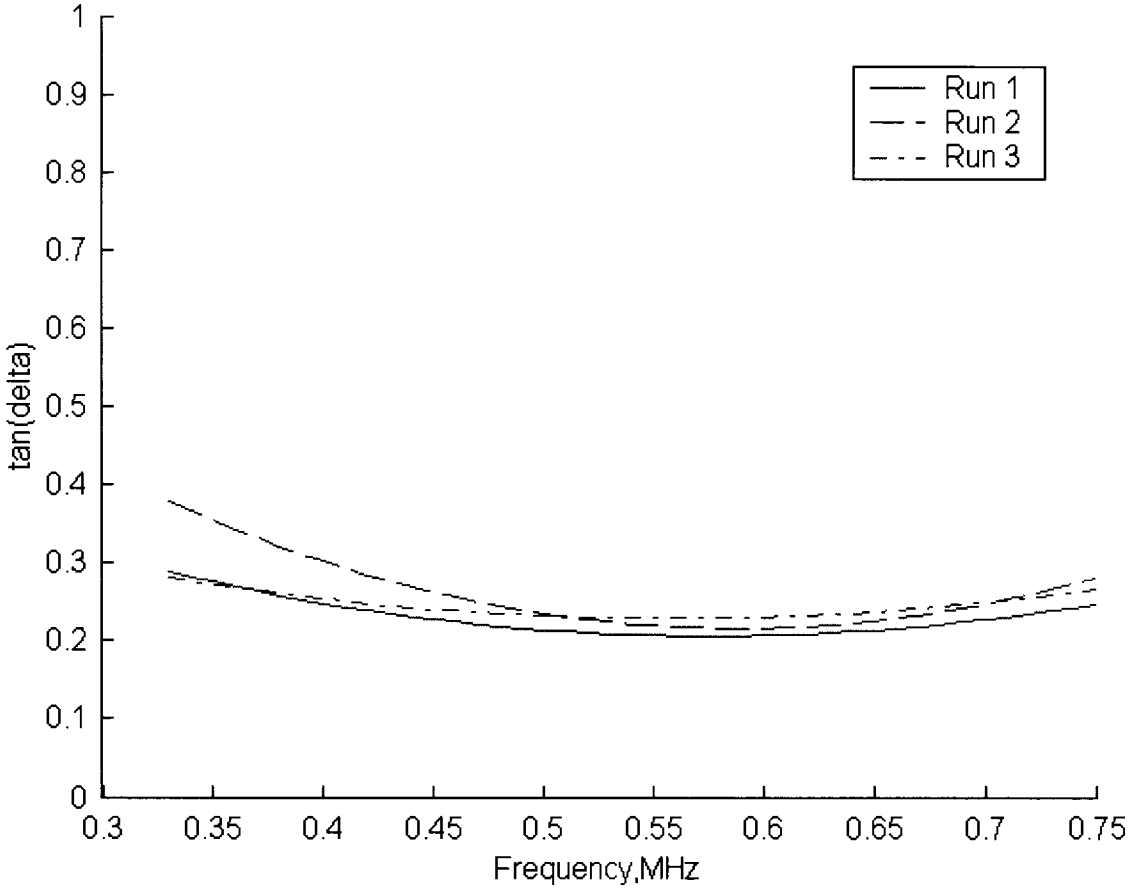

Figure B.4 Smoothened curve showing repeatability of damping characterization process, over 3 different runs on 3 different days under same conditions and same orientation for e-glass vinylester

		Dimensions before oxidation (m)		
Sample No:	Weight before oxidation (g)	Length	Breadth	Thickness
1	5.89	0.01882	0.01781	0.00937
2	5.89	0.01882	0.01781	0.00937
3	5.73	0.01905	0.01854	0.00841
4	5.55	0.01867	0.01854	0.00851
5	7.59	0.02057	0.02029	0.00978
6	7.62	0.02032	0.02007	0.00996

Oxidation time (min)	Weight after oxidation (g)	Weight Loss	Percentage Loss in weight	Thickness after oxidation
0	5.89	0.0	0.00%	0.00937
45	5.76	0.1	2.21%	0.00937
45	5.43	0.3	5.24%	0.00841
45	5.17	0.4	6.85%	0.00851
45	7.05	0.5	7.11%	0.00978
45	6.01	1.6	21.13%	0.00996

Actual difference in tandelta				
0.33 MHz	0.50 MHz	0.63 MHz	0.70 MHz	0.75 MHz
0.0634	0.1263	0.1377	0.1771	0.3192
0.0954	0.0399	0.2800	0.4510	0.1631
0.1053	0.0175	0.1666	0.4288	0.3228
0.1075	0.0183	0.1457	0.2633	0.2560
0.0215	0.0233	0.0167	0.1419	0.1090
0.0536	0.0617	0.0129	0.0919	0.0503

Table B.1 Raw data for Figure 6.5, attenuation changes during oxidation

BIOGRAPHY OF THE AUTHOR

Anish Sen Senan was born in Trivandrum, Kerala, India on November 1, 1976. He was raised in Trivandrum and graduated from Kendriya Vidyalaya High School in 1992. He attended the College of Engineering, Trivandrum (University of Kerala) for his Bachelor's degree in Mechanical Engineering. He earned his Bachelor's in Technology (B.Tech) degree in 1998. After graduation he worked as Materials-Engineer, at Wipro Computers Ltd, India for 2 years. Later in 2000 he joined Acclaim Systems, Inc as Business Development Manager. He came to the United States of America in 2001 and started his graduate program in December 2001.

Anish is a candidate for the Master of Science degree in Mechanical Engineering from The University of Maine in December, 2003.